DISSERTATION APPROVED BY

May 7, 2020

Date

Thomas F. Murray, Ph.D., Chair

Peter W. Abel, Ph.D.

Shashank Dravid, Ph.D.

Roselyn D. Cerutis, Ph.D.

Gail M. Jensen, Ph.D., Dean

SODIUM CHANNEL GATING MODIFIER PROMOTES NEURONAL REPAIR AND FUNCTIONAL RECOVERY FROM ISCHEMIC STROKE.

By

ERICA SEQUEIRA

A DISSERTATION

Submitted to the faculty of the Graduate School of the Creighton University in Partial Fulfillment of the Requirements for the degree of Doctor of Philosophy in the Department of Pharmacology and Neuroscience

Omaha, NE

(May 7, 2020)

Abstract

Ischemic stroke is a leading cause of adult disability, which presents a pressing need for a pharmacological therapy. Emerging literature suggests that after a stroke, the peri-infarct region exhibits dynamic changes in excitability. The acute ischemic phase triggers glutamate-mediated excitotoxic neuronal death. On the contrary, during the chronic phase, when the brain begins to repair itself, it displays heightened neuroplasticity that also resembles the neuronal developmental stages. However, this recovery is incomplete. Thus, promoting cortical excitability during the repair and recovery phase could potentially be therapeutic. Brevetoxin-2 (PbTx-2), a voltage-gated sodium channel (VGSC) modifier, increases intracellular sodium ($[Na^+]_i$), upregulates *N*-methyl-d-aspartate receptors (NMDAR) channel activity, and engages activity-dependent downstream calcium (Ca^{2+}) signaling pathways. In immature cerebrocortical neurons, PbTx-2 promoted neuronal structural plasticity by increasing neurite outgrowth, dendritogenesis and synaptogenesis. This led us to hypothesize that PbTx-2 could promote structural remodeling of neural networks in the peri-infarct site and subsequently promote functional outcomes after stroke. In the current study, we have investigated this phenomenon using adult male transgenic yellow fluorescent protein expressing (YFP) mice by providing an epicortical application of PbTx-2 five days after inducing a photothrombotic stroke. We show that PbTx-2 enhanced dendritic arbor complexity and excitatory synapse density of the cortical layer V pyramidal neurons in the peri-infarct cortex. Consistent with increased neuronal plasticity, PbTx-2 also produced a robust gain of motor recovery. Collectively, our results identify an activity-dependent pharmacologic strategy to promote recovery from stroke and possibly other brain injuries.

Acknowledgements

I am indebted to my parents *Richard* and *Honorata Sequeira* who encouraged my dream to pursue my doctorate degree at Creighton University. I am very grateful for all the support you have provided from kindergarten, to college, and to graduate school. Thank you to Kyle Purcell, for being such a great husband/best friend and my two cats Chester and Felicia. I love you all.

Special thanks to *Dr. Thomas Murray* for all his patience, encouragement and mentorship during this journey. I will always appreciate the faith he had in me, which led me to persevere and do my best.

I would also like to thank *Dr. Peter Abel, Dr. Shashank Dravid* and *Dr. Roselyn Cerutis*, my committee members for their guidance and willingness to help in my project. I appreciate their insights and words of advice very much.

Thank you to *Dr. Marsha Pierce, Bridget Sefranek, Dr. Dina Akasheh, Dr. Suneet Mehrotra* and *Stacey Sigmon* for being patient and teaching me everything they knew.

Finally, thank you to the Department of Pharmacology and Neuroscience, my fellow graduate students, and to Creighton University, my home for five years. *Go Jays!*

CONTENTS

List of Figures

List of Tables

List of Abbreviations

AMPA	α-amino-3-hydroxy-5-methylisoxazole-4-propionic acid
AUC	area under the curve
BDNF	brain-derived neurotrophic factor
CaMKs	Ca2+-calmodulin kinases
CNS	central nervous system
CREB	cAMP response element binding protein
CS	cryptogenic stroke
CT	computerized tomography
DMSO	dimethyl sulfoxide
ERK	extracellular-signal-regulated kinase
GABA	γ-aminobutyric acid
IP	intraperitoneal
JNK	c-Jun N- terminal protein kinase
LF	left front

LH	left hind
MAPK	mitogen-activated protein kinase
MCAO	middle cerebral artery occlusion
MRI	magnetic resonance imaging
[Na+]I	intracellular sodium
NMDA	N-methyl-d-aspartate
NMDAR	N-methyl-d-aspartate receptor
NMDG	N-methyl D-glucamine
rt-PA	recombinant tissue plasminogen activator
PbTx-2	brevetoxin-2
PBS	phosphate-buffered saline
PFA	paraformaldehyde
PNS	peripheral nervous system
PSD-95	postsynaptic density 95
PTK	phosphotyrosine kinases
PTP	phosphotyrosine phosphatases

PTS	photothrombotic stroke
RF	right front
RH	right hind
SMZ/TMP	sulfamethoxazole and trimethoprim
SFK	**S**rc family kinases
TIA	transient ischemic attack
tPA	tissue plasminogen activator
TrkB	tropomyosin-related kinase B
VGLUT1	vesicular glutamate transporter 1
VGSC	voltage-gated sodium channel
YFP	yellow fluorescent protein expressing

CHAPTER 1: INTRODUCTION AND REVIEW OF THE LITERATURE

Stroke epidemiology

Stroke is one of the leading causes of mortality and adult disability worldwide. Although the rate of stroke mortality has decreased in high-income countries, no significant difference has been seen in low and middle-income countries. Globally, stroke is the second leading cause of death [Mozaffarian et al., 2016]. Stroke also has an annual economic cost of approximately $34 billion worldwide (Mozaffarian et al., 2015). Stroke affects more than 795,000 people each year with nearly 1 of 4 occurring in people who have had a previous stroke (Benjamin et al., 2017).

In the United States, the geographic disparities are dramatic. Mortality is 20% higher in the stroke belt, identified as South Carolina, North Carolina, Georgia, Tennessee, Louisiana, Mississippi, Alabama and Arkansas (Howard et al., 1997). This is mostly attributed to socioeconomic status and regional differences in culture such as cigarette smoking and consumption of high salt and fat food.

Types of stroke

Ischemic stroke

Ischemic stroke accounts for 87% of all strokes (Donnan et al., 2008) and is caused by interruption of blood supply to a part of the brain resulting in a sudden loss of function. Ischemic strokes are further classified into thrombotic or embolic strokes.

Thrombotic strokes are caused by a blood clot that forms in and occludes blood vessels inside the brain. Embolic strokes are caused by a clot or plaque that travels from somewhere in the body and then blocks one of the blood vessels in the brain.

Hemorrhagic stroke

Hemorrhagic strokes are commonly caused by hypertension, anti-coagulation therapy, cerebral amyloid angiopathy, and vascular structural lesions (Rannikmae et al., 2016). Intracerebral hemorrhage occurs when a blood vessel within the brain bursts, causing blood to leak inside the brain. This type of hemorrhage usually occurs in the cerebellum, brain stem, basal ganglia or cortex. Subarachnoid hemorrhage occurs when a blood vessel on the surface of the brain bursts and bleeds into the space between the brain and the skull (subarachnoid space).

Transient Ischemic Attack

Transient Ischemic Attack (TIA) is often called a mini- stroke but is a warning sign for a major stroke. TIA occurs due to a temporary blockage of blood flow to the brain. The body usually responds by moving the clot downstream or by use of endogenous anticoagulants in the blood. According to the American Stroke Association, 15% of stroke patients have a TIA history and up to 25% of people with TIA die within a year. Approximately one-third of patients with TIA progress to a more severe stroke within one year of onset.

Cryptogenic Stroke

A stroke of unknown cause is called a Cryptogenic Stroke (CS). There are several different definitions of CS. The Trial of Org 10172 in Acute Stroke Treatment defines CS as a cerebral infarct not attributed to a definite source of cardioembolism, large-vessel atherosclerosis, or small-vessel disease, despite:

(1) extensive cardiac, vascular, hematologic, and serological evaluation;

(2) evidence of > 1 competing cause, or

(3) incomplete diagnostic evaluation (Adams et al., 1993).

In most situations, the cause of CS is unknown because it is transitory or reversible or in some cases the causes remain unknown. Statistically, about one third of ischemic strokes are classified as cryptogenic and is predominantly detected in younger compared to older patients due to cardiac embolism, followed by coagulopathy and vasculopathy. Cardiac embolism occurs due to an embolism from upstream veins from patent foramen ovale, valvular disease, atrial septal aneurysm, and atrial fibrillation (Finsterer, 2010).

Brain Stem Stroke

According to the American Stroke Association, patients with brain stem strokes can display complex symptoms making it difficult to diagnose. For example, a patient may have vertigo, dizziness and severe imbalance without the characteristic symptom of stroke- weakness on one side of the body. A brain stem stroke can also present itself with other symptoms such as slurred speech, double vision and decreased level of consciousness. The brain stem controls several important activities of such as consciousness, breathing, motor control and blood pressure. A severe brain stem stroke can also cause a lock-down syndrome, in which survivors can only move their eyes and are generally unable to speak or move below the neck. Risk factors for brain stem stroke are similar as strokes in other areas of the brain. Other rare causes include injury to an artery due to sudden head or neck movements.

Diagnosis of stroke

Depending on the area of brain damage, patients experience sudden unilateral paralysis, altered speech, vision loss, ataxia, visual-spatial-perceptual dysfunction (M.A Moskowitz 2010). Stroke subtypes are determined using Computerized Tomographic (CT) imaging or Magnetic Resonance Imaging (MRI). CT scans are most commonly used, whereas MRI gives more accurate information and can distinguish between hemorrhage and a thrombus (Merino and Warach, 2010).

Risk factors

Genetic Risk Factors

Genome wide association studies have identified a wide range of pathophysiological genes associated with stroke occurrence. Some of these include Endothelial Nitric Oxide Synthase (ENOS), Apolipoprotein E (APOE), Cytochrome P450 4F2 (CYP4F2), methylenetetrahydrofolate reductase (MTHFR), Factor V Leiden (F5), beta-fibrinogen, and Phosphodiesterase 4D (PDE4D) (Auer et al., 2015; Carty et al., 2015; Gretarsdottir et al., 2008; Ikram et al., 2009).

Other risk factors

Traditional risk factors of stroke can be classified into modifiable and unmodifiable risk factors. Modifiable risk factors include, hypertension, hypercholesterolaemia, atrial fibrillation, and carotid artery disease, alcohol consumption, cigarette smoking, physical inactivity and diabetes mellitus. Nonmodifiable risk factors include age and gender (Odonnell et al.,2010; Lopez et al., 2006]. Risk of suffering from stroke increases by age, but strokes can occur at any age. In the year 2009, 34% of stroke patients were under the age of 65 (Hall et al., 2012).

Current treatment strategies

Depending on timing, there are 3 broad treatment stages for stroke: prevention, therapy immediately after the stroke, and post-stroke rehabilitation. Therapies to prevent a first or recurrent stroke are based on treating a patient's underlying risk factors for stroke. Acute stroke therapies try to stop a stroke while it is happening by quickly dissolving or removing the blood clot or by stopping the bleeding in the case of a hemorrhagic stroke. Post-stroke rehabilitation therapy helps patients overcome disabilities that result from stroke damage.

Antithrombotics

Antithrombotics include antiplatelet agents and anticoagulants. Antiplatelet drugs prevent clotting by decreasing platelet activity that contributes to blood clotting and are mainly prescribed for stroke prevention. These include aspirin, clopidrogel, dipyridamole, and ticlopidine. Anticoagulants reduces blood clotting. Most commonly used anticoagulants include warfarin, heparin, and enoxaparin (NINDS, 2004).

Thrombolytic agents

Thrombolytic agents are used to treat an ongoing acute ischemic episode caused by a blocked artery. Recombinant tissue plasminogen activator (rtPA), a genetically engineered form of tPA can be effective if provided intravenously within 3 hours of stroke onset, resulting in only 3-9% of patients that received the treatment (Chang and Prabhakaran, 2017). The ECASS-3 trial in 2008 recently extended r-tPA eligibility from 3 to 4.5 hours, with additional exclusion criteria, thereby increasing r-tPA utilization by 20% in some medical centers (Lyerly et al., 2013)

Surgery

The introduction of endovascular therapy further expanded the treatment window to up to 7 hours from stroke onset in select patients (Table 1). The American stroke Association/ American Heart Association has published selection criteria for endovascular therapy for patients with acute ischemic stroke (Powers et al., 2015).

Acute ischemic stroke receiving t-PA within 4.5 hours of stroke onset.
Stroke caused by occlusion of proximal or middle cerebral artery or internal carotid artery.
Treatment to be initiated within 6 hours of stroke onset.
NIH stroke scale/ score of >- 6
Functionally independent before stroke (modified Rankin score of 0 to 1)
Age >- 18 years

Table 1- America Heart Association selection criteria

Extracranial/ Intracranial (EC/IC) bypass surgery is a procedure that restores blood flow to the area of the brain tissue that is compromised by rerouting a normal artery to the damaged brain tissue. However, EC/IC is not beneficial in the long run and is occasionally used for aneurysms or certain types of vascular deformities.

Rehabilitation Therapy

Physical therapy (PT) promotes relearning simple motor movements such as standing, sitting, walking, lying down, and switching from one movement to another. It includes training, exercises and physical manipulation of the patient in order to restore movement, balance and coordination. Occupational therapy (OT) aims to facilitate patients to become more independent. OT also involves training the patients to help relearn daily activities such as eating, drinking, cooking, bathing, reading and writing (NINDS, 2004).

Excitotoxicity associated with ischemic stroke

During ischemia, restricted blood vessel results into depletion of oxygen and essential nutrients required for maintenance of ionic homeostasis and results in triggering the release of the excitatory neurotransmitter- glutamate (Dirnagl et al., 1999). Additionally, energy depletion also disrupts the re-uptake transporters and results in accumulation of glutamate in the synaptic space. Ionotropic glutamate receptors are ligand-gated ion channels that allow rapid ion influx in response to glutamate and are broadly classified into two main subtypes: NMDA (N-methyl-d-aspartate) receptors (NMDARs) and AMPA (α-amino-3-hydroxy-5-methylisoxazole-4-propionic acid) receptors (AMPARs). Normally, in the resting state, the NMDA channels are blocked by

Mg^{2+}. When glutamate is released from pre-synaptic sites, activated AMPARs cause a partial depolarization sufficient to remove the Mg^{2+} block from NMDARs. Once NMDARs are activated, they cause influx of Na^{+} and Ca^{2+} into the cell. However, during excitotoxicity, excess glutamate release results in over-activation of NMDARs and leads to calcium overload inside the neurons. Excess calcium triggers a cascade of downstream signaling events such as calpain activation [Curcio, 2016; Xu J, 2009], reactive oxygen species generation (Kristian and Siesjo, 1998; Eliasson, 1999; Lau and Tymianski, 2010), and mitochondrial damage (Kristian and Siesjo, 1998), ultimately resulting in cell death.

Zones of stroke damage

Infarct core

The core denotes the part of the ischemic tissue which is permanently infarcted due to acute loss of blood flow and is destined to infarct regardless of reperfusion. Loss of blood flow precipitates a cascade of excitotoxic events that directly damage the parenchyma of the brain including the neurons, blood vessels, astrocytes, oligodendrocytes, microglia, and oligodendrocyte precursor cells.

Peri-infarct region

Peri-infarct is the tissue adjacent to the infarct core and has experienced partial damage that risks progressing to infarction but is still potentially salvageable. The partial blood supply triggers endothelial cells to localize neutrophils and macrophages. Additionally, activation of astrocytes triggers the production of cytokines, matrix metalloproteases and chondroitin sulfate proteoglycans that cause secondary damage, but also generate signals for neuronal repair such as promoting angiogenesis, axonal sprouting; and synchronized neuronal activity that promotes the formation of new connections (Carmichael, 2016).

Neuroplasticity

Neuroplasticity is broadly defined as the ability of the nervous system to adopt a new structural or functional state in response to extrinsic and intrinsic factors (Ganguly and Poo, 2013). Plasticity plays a key role not only in the normal process of learning, memory and adaptation, but also in response to ischemic stroke and other central nervous system (CNS) injuries (Boller 2004). Mechanisms involved in post-stroke recovery are similar to those involved in the development of the nervous system. Two factors that enable post-stroke plasticity in an adult brain are (1) redundant connectivity in the CNS, (2) formation of new structural and functional circuits through remapping of related cortical areas. (Murphy and Corbett, 2009). It has also been suggested that although the brain has a defined circuitry, it functions as a spatially distributed system that signals through multiple pathways and is capable of adapting to changes in signal transmission.

As mentioned earlier, the brain has the capacity to alter the structure and function of neurons in response to changing demands. Therefore, when a normal input to a cortical area is lost due to injury, rapid structural and functional reorganization results in activation of this area by the surrounding intact regions. For instance, in macaque monkeys, recovery of dexterity after a unilateral stroke is mediated by the ipsilateral hemisphere (Liu and Rouiller, 1999). Similarly, in humans, recovery in patients is associated with increased activity in the ipsilateral cortex (Gerloff et al., 2006). This process of remapping occurs with changes in neuronal excitability where an initially less responsive peri-infarct area or zone displays a differential return of neuronal activation (Lim et al., 2014). Recovery in smaller strokes (those that affect 5 to 15 % of tissue) involves the peri-infarct area that performs similar functions (Brown et al., 2009). In contrast, for larger strokes, tissues with similar functions are founds at more distant regions or even the contralateral hemisphere (Biernaskie et al., 2005). Recovery achieved through cortical reorganization in the contralateral region is associated with compensation whereas recovery involving the peri-infarct area is associated with true recovery.

The neurobiological recovery post-stroke can be divided into 5 phases. (1) hyper-acute: 0 to 24 hours, (2) acute: 1 to 7 days, (3) early subacute: 7 days to 3 months, (4) late subacute: 3 to 6 months, and (5) chronic: 6 months and more (Fig. 1).

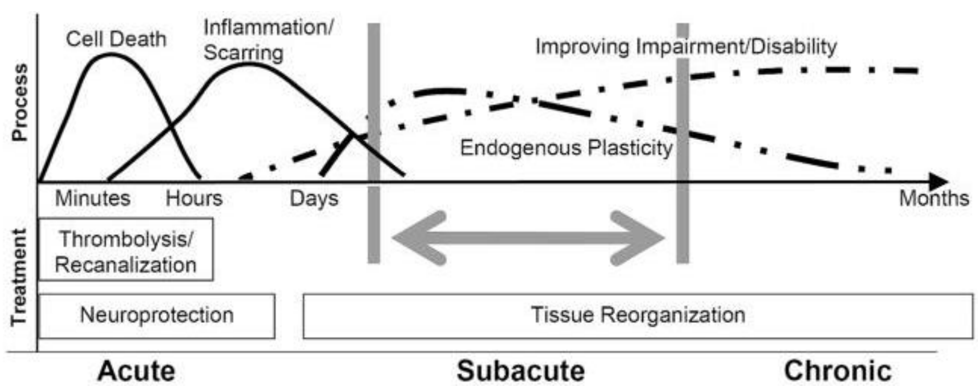

Figure 1- Progression of stroke damage, tissue reorganization and behavioral recovery (Dobkin and Carmichael, 2016).

Brain excitability during ischemic stroke

Neuronal excitability after a stroke exhibits a yin and yang phase, where the acute phase is deleterious and is characterized by neuronal depolarization, excessive glutamate and calcium levels, and excitotoxicity. Due to elevated excitability during the acute phase, blocking glutamate or enhancing GABA signaling promotes neuroprotection, in animal models of stroke. However, during the chronic phase (Fig. 2), the peri-infarct tissue displays a marked increase in extracellular γ-aminobutyric acid (GABA) levels due to the loss of the GABA transporter GAT-3(Clarkson et al., 2010). Notably, administration of L655,708, a benzodiazepine inverse agonist specific to the extrasynaptic $GABA_AR$, produced early and sustained functional gains. Additionally, increasing baseline glutamatergic excitability during the chronic phase through direct current stimulation of the peri-infarct region improved the use of the affected limb in patients after stroke (Hummel and Cohen, 2006). Hence, counteracting the hypo-excitability caused by heightened inhibition, could potentially promote recovery when initiated during the chronic phase. This inflection point from acute to chronic phase has been reported to occur 3 days after stroke in mice.

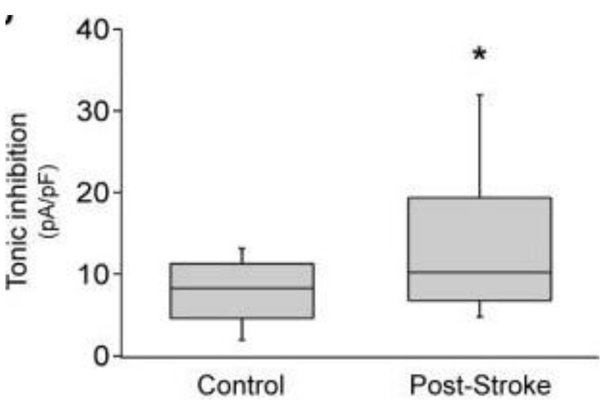

Figure 2 - Boxplot showing elevated tonic inhibition post-stroke in the peri-infarct region. Whole-cell-patch-clamp recordings obtained from post-stroke brain slices, within peri-infarct region (Clarkson et al., 2010).

Voltage-gated sodium channels (VGSC)

VGSCs play an essential role in action potential initiation and propagation, they mediate forms of synaptic plasticity that depend on neuronal firing (Cantrell and Catterall, 2001). Sodium currents were first recorded by Hodgkin and Huxley using the voltage clamp procedure, showing the key features such as voltage gated activation, rapid inactivation (1-2 milliseconds) and selective ion conductance to sodium (Hodgkin and Huxley, 1952). Structurally, the VGSC consists of a pore-forming α subunit, which can function independently, together with 1–4 auxiliary β subunits (Wood, 2001; Yu and Caterall, 2003; Yu et al., 2005; Caterall, 2000). To date, 10 VGSC subtypes have been identified in mammals. They were named Nav1.1-Nav1.9 and NavX based on differences in the α subunit (Yu and Caterall, 2003; Yu et al.,2005; Goldin et al., 2000). VGSCs are composed of 4 transmembrane domains (DI-DIV); 3 intracellular loops (L1, L2 and L3); and the N-terminus and C-terminus (NT and CT) (Fig, 3). Further, each transmembrane domain contains 6 α-helical transmembrane segments (S1-S6). The transmembrane segment S4 is called the “voltage sensor” as it is extremely sensitive to changes in membrane potential. The intracellular loop L3 between the domains DIII and DIV has 3 amino acid residues and is involved in rapid inactivation of the channel (Yu FH 2003).

VGSC α subunits are distributed differently in the CNS and peripheral nervous system (PNS). Nav1.1, Nav1.2, Nav1.3, Nav1.5, and Nav1.6 Na^+ channels are more widely distributed in the CNS, whereas the Nav1.7, Nav1.8, and Nav1.9 Na^+ channels are predominantly distributed in the PNS (Candenas et al., 2006; Vacher et al., 2008; Pappalardo et al., 2016; Lai and Jan, 2006; Whitaker et al., 2000; Wang et al., 2009; Onkal et al., 2008; Whitaker et al., 2001; Fukuoka and Noguchi, 2011; Schaller and

Caldwell, 2000 and 2003). VGSCs have three characteristic features: (1) voltage-dependent activation; (2) rapid inactivation; and (3) Na^+ selectivity (Wood and Baker, 2001; Yu and Caterall, 2003; Goldin et al., 2000; Diss et al., 2004). VGSCs switch between 3 states depending on the membrane potential. In excitable cells, depolarizations cause a rapid rise in Na^+ permeability due to opening from their resting state. This process involves voltage sensors to move in an outward direction due to the change in membrane potential. This increase in Na^+ permeability causes membrane depolarization that characterizes the initial phase of the action potential.

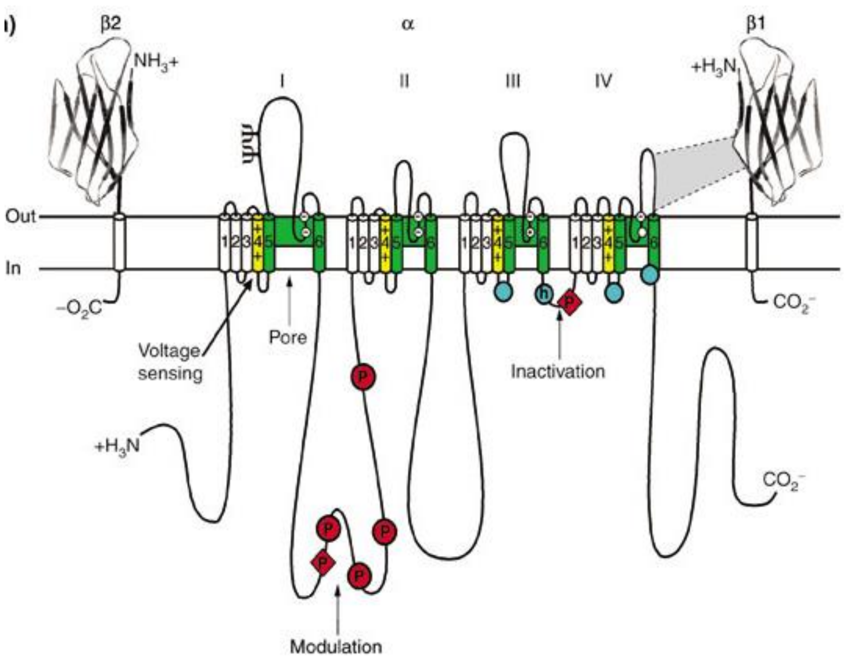

Figure 3 - The voltage-gated sodium channel [Yu FH, 2003].

N-methyl-d-aspartic acid (NMDA)

Excitatory synaptic transmission is primarily mediated by the amino acid glutamate that activates 2 groups of glutamatergic receptors: ionotropic and metabotropic. Ionotropic receptors are further classified into α-amino-3-hydroxy-5-methyl-4-isoxazolepropionic acid receptor (AMPA), kainite, N-Methyl-D-aspartic acid (NMDA), and delta receptors. Structurally, the NMDA receptors consists of GluN1-3 subunits. GluN2 and N3 are encoded by 4 (GluN2A-D) and 2 (GluN3A and B) genes, respectively (Monyer et al., 1992). Functional NMDA receptors are organized as heterotetramers containing GluN1 subunits in combination with 2 GluN2 and/ or GluN3 subunits (Monyer et al., 1992, Ulbrich and Isacoff, 2008). The amino terminal domain is linked to the ligand binding domain, which in turn is connected to the transmembrane domain, thus forming an ion channel. This structure in turn communicates with the carboxy-terminal domain (Traynelis et al., 2010). In terms of channel gating, NMDA receptors require the simultaneous binding of 2 ligands for receptor activation: 2 molecules of the agonist glutamate (Watkins and Evans, 1981, Patneau et al., 1990; Clements and Westbrook, 1991) and 2 molecules of the coagonist glycine (Johnson and Ascher, 1987; Kleckner and Dingledine, 1988). Once glutamate is released from the presynaptic nerve it reaches a peak cleft concentration of approximately 1mM and is then rapidly removed by diffusion/uptake (Bergles et al., 1999). The transient glutamate concentration results in a normal synaptic transmission via activation of NMDA receptors. However, disease states are associated with dysregulated glutamate release or uptake (Mattson 2003, Nyitrai et al., 2006), therefore resulting in an extended elevation of glutamate levels reaching μM values (Heinrich et al., 2012, Phillis and O'Regan, 2003). This results in excitotoxic tonic activation of NMDA receptors.

NMDA receptors play a pivotal role in synaptic plasticity (Collingridge, 2004). Physiological activation of NMDA receptors during development can promote neuronal survival, migration and dendritic outgrowth (Pearce et al., 1987; Komuro and Rakic, 1993). However, excessive NMDA receptor activity leads to neuronal necrosis that occurs in the ischemic core of a stroke (Bonfoco et al.,1995) (Fig. 4).

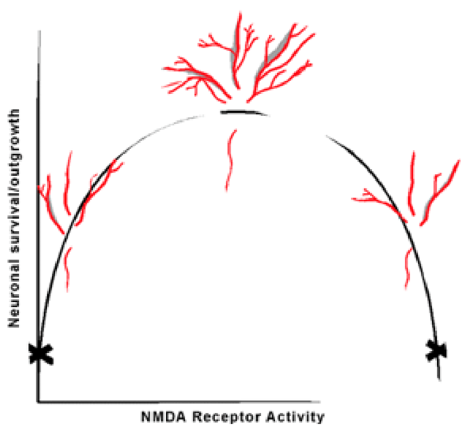

Figure 4 - Graph depicting an inverted U-shaped dose-response relationship of NMDA receptor activity versus neuronal survival and outgrowth. Too little or excessive NMDA receptor activity results in neuronal death (Lipton and Nakanishi, 1999).

Brevetoxin (PbTx)

Brevetoxins (PbTx-1 to PbTx-10) are potent lipid-soluble polyether neurotoxins produced by the marine dinoflagellate *Karenia brevis* (formerly known as *Gymnodinium breve* and *Ptychodiscus brevis*), an organism linked to periodic red tide blooms in the

Gulf of Mexico along the western Florida coastline (Baden, 1989) and New Zealand (Ishida et al, 1995). Although brevetoxin toxicity can result from inhalation, oral or dermal exposure, the most common route of exposure is by ingestion of contaminated shellfish. Neurotoxic Shellfish Poisoning is characterized by paresthesia, vertigo, reversal of temperature, myalgia and ataxia. Other symptoms include gastrointestinal discomfort such as abdominal pain, diarrhea and nausea (Morris et al., 1991). Inhalation exposure may cause respiratory symptoms characterized by bronchospasm, dyspnea, and cough (Tunik, 2011; Baden et al., 2005; Fleming et al, 2005; Watkins et al., 2008).

Structurally, PbTx-2 is composed of three distinct regions: H-K ring system, an A-ring lactone, and a B-G ring region (Fig. 5). All active forms of the toxins, whether they are members of the brevetoxin A or brevetoxin B backbone, possess these characteristics (Gawley et al., 1995).

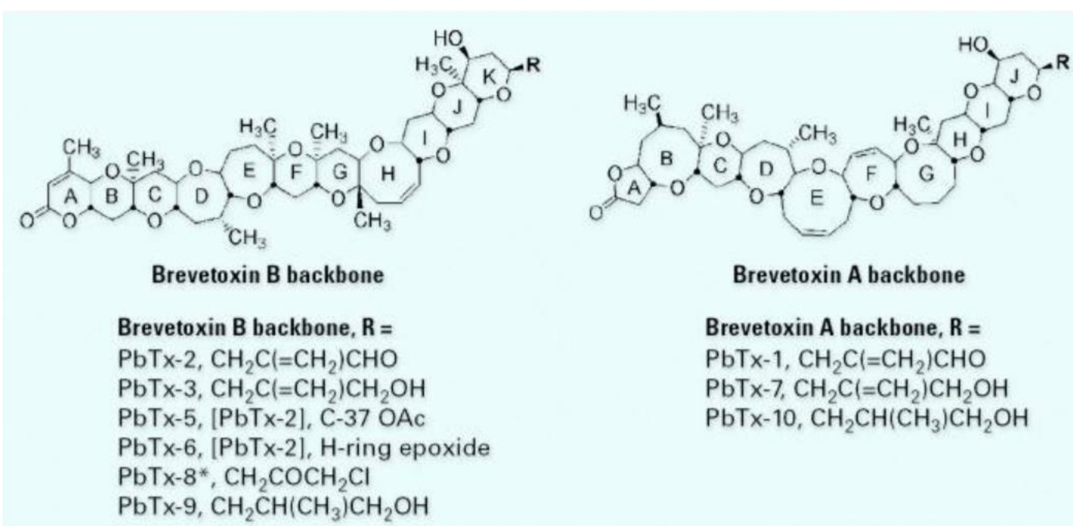

Figure 5 - Structural backbones of brevetoxin. [Baden et al., 2005]

Type A brevetoxins such as PbTx-1, 7, and 10, are more potent than type B, however, are less stable and of limited supply (Poli et al., 1986). Of the type B PbTxs, PbTx-2 is the major naturally occurring PbTx produced with successively lower amounts of PbTx-3 followed by PbTx-1. Karenia brevis produces type B PbTxs in an approximate ratio of 20:4:1, respectively (Poli et al., 2000). The active toxin binds at site 5 of the α subunit in a "head-down" orientation, intercalating between domains DIII and DIV (Poli et al.,1986; Gawley et al.,1995 and Trainer et al., 1994). Brevetoxins interact with site 5 of the α-subunit of the VGSC. Brevetoxins augment Na^+ influx through VGSC by increasing the mean open time of the channel, inhibiting channel inactivation and shifting the activation potential to more negative values (Jeglitsch et al, 1998).

Pbtx-2 augments NMDAR function

Studies have reported that intracellular sodium concentrations may act as a signaling molecule and play a role in activity-dependent plasticity as indicated by increased $[Na^+]_i$ increments in the dendrites and spines during synaptic stimulation (Rose et al., 1999; Rose and Konnerth, 2001). Additionally, Src family kinases (SFKs) are widely expressed in the CNS and play an important role in regulating activities of ion channels such as the NMDARs. They also regulate other types of channels in neurons including voltage-gated ion channels, such as calcium and potassium, as well as GABAA (gamma-aminobutyric acid type A) receptors and nicotinic receptors. Electrophysiological studies have shown than NMDA currents are regulated by a balance between tyrosine phosphorylation and dephosphorylation. Protein tyrosine kinase (PTK) inhibition or increasing phosphotyrosine phosphatases (PTP) leads to suppression of NMDAR currents. Conversely, NMDAR currents are increased by increasing PTK activity or inhibiting PTP activity. Tyrosine phosphorylation by Src facilitates the binding of Na+ to NMDAR and exerts a regulatory effect on NMDAR signaling (Salter, 1999).

Previous studies (George et al., 2009) have demonstrated that PbTx-2 exposure leads to augmentation of NMDA receptor signaling and this effect was mediated by an increase in Src kinase activity and increased intracellular [Na^+]. Membrane potential assays indicated that PbTx-2 augmentation of NMDA receptor signaling does not involve depolarization-induced relief of Mg^{2+} blockade. Single-channel currents from cell-attached patch clamp recordings demonstrated that PbTx-2 induced upregulation of NMDAR was mediated by increased open probability and mean open time of NMDARs. Further analysis to demonstrate the requirement of Na^+ used PbTx-2 applied when Na^+ was substituted by an impermeable cation N-methyl D-glucamine (NMDG). Under these conditions, PbTx-2 failed to upregulate NMDAR function. Resubstituting back with Na^+ caused PbTx-2 to significantly increase the mean open time and open probability of NMDARs, thus suggesting the requirement of Na^+ for augmenting NMDAR function. Previously the same group also found that PbTx-2 augmented NMDAR-mediated Ca^{2+} influx in both mature and immature neurons (Dravid et al., 2005)

PbTx-2 engages downstream activity-dependent signaling mechanisms

Mitogen-activated protein kinases (MAPK) are activated by phosphorylation of tyrosine and threonine that convert extracellular stimuli into intracellular responses. Major MAPK signaling cascades include extracellular signal-regulated kinases (ERK1/2), c-Jun N- terminal protein kinase (JNK), and p38 (Cargnello and Roux, 2011). Of this family, the most studied, ERK1/2, plays an important role in cell survival. Upon activation ERK translocates into the nucleus and phosphorylates transcription factors that are involved in regulating gene expression (Chang et al., 2003), and facilitating DNA synthesis (Dangi et al., 2006). ERK1/2 phosphorylates cAMP responsive element binding protein (CREB) which regulates the transcription of several genes including brain-derived neurotrophic factor (BDNF). Binding of PbTx-2 to VGSC's leads to increases in intracellular calcium levels in neurons, thus triggering the activation of ERK 1/2 (Dravid et al., 2004). Further, ERK1/2 activation was shown to be mediated by calcium influx through NMDA receptors; when these receptors were blocked by MK-801, the ERK 1/2 expression was significantly reduced suggesting the underlying role of NMDA. CREB activation mediates activity-dependent dendritic arborization and PbTx-2 stimulation of CREB phosphorylation at Ser 133 iss also NMDA dependent. BDNF is one of the most well-known molecules associated with activity-dependent plasticity and has been shown to promote functional recovery in preclinical models of stroke (Schabitz et al., 2007 and Takeshima et al., 2011). BDNF signaling is increased in the peri-infarct region and mediates motor recovery in cortical strokes (Clarkson et al., 2011). PbTx-2 exposure increased cell surface expression of BDNF-tropomyosin-related kinase B (TrkB) receptors. TrkB receptors have been shown to have profound neurotrophic effects in the developing and mature nervous system, and the surface expression of TrkB is neuronal activity dependent (Du et al., 2000). The GluN2 B subunit is a predominant subunit of NMDARs and regulates surface expression of these receptors (Groc et al., 2006). Exposure of cerebrocortical neurons to PbTx-2 significantly increased the cell surface expression of GluN2B subunits.

PbTx-2 promotes neurite outgrowth

Dendritic filopodia are protrusions found predominantly in the developing brain that evolve into mature dendritic spines (Ziv and Smith, 1996). In vitro studies in cerebrocortical neurons show that PbTx-2 enhanced total protrusion density as compared to controls. Additionally, PbTx-2 exposed cerebrocortical neurons displayed a significant shift from long to stubby-type filopodial protrusions. Long filopodia are considered to be immature and stubby shaped filopodia are referred to as the mature form of filopodia (Portea-Cailliau et al., 2003). Additionally, these effects were antagonized with TTX and APV but not nimodipine. Thus, indicating PbTx-2 effect on total filopodia density and maturation and that NMDARs play an essential role in expansion of dendritic arbors mediated through Ca^{2+}-dependent signaling (Wong and Ghosh, 2002; Konur and Ghosh, 2005).

PbTx-2 produced a robust increase in dendritic arbor complexity and this effect was attenuated by pharmacological inhibitors such as TTX and MK801, but not nimodipine (L-type calcium channel blocker). This suggests that PbTx-2 activation of VGSC induced enhancement of NMDA receptor signaling is responsible for dendritic arborization.

Animal models of ischemic stroke

No single animal model mimics all aspects of a human stroke because ischemic stroke is a heterogeneous disorder with a complex pathophysiology. Hence selecting an appropriate animal model to optimize the study design can improve the translational potential of animal model studies (Table 2).

Model	**Description**
Middle cerebral artery (MCA) occlusion model	Interrupts MCA by use of suture, mimics human stroke, increased hemorrhage thus not suitable for thrombolysis studies.

Craniotomy model	MCA occlusion requiring craniotomy, good reproducibility, highly invasive causing injury of underlying cortex and vessels, disrupting BBB and intracranial pressure.
Photo thrombosis model	Intravascular photo-oxidation, localized lesions, highly reproducible, low invasiveness, used to study neuroprotective drugs, can cause cytotoxic damage and vasogenic edema.
Endothelin-1-model	Application of vasoconstrictive peptide: endothelin-1, low invasiveness, duration of ischemia is uncontrollable.
Embolic stroke model	Mimics pathogenesis of human stroke, used for study of thrombolytics or neuroprotective drugs, variability in lesion and uncontrollable reperfusion.

Table 2 - Animal models of ischemic stroke. (Felix Fluri et al., 2015)

Photothrombotic stroke

The photothrombotic stroke model aims to induce ischemic damage within the cortical area of interest by means of photo-activation of a previously injected light-sensitive dye. Post illumination, the dye is activated and generates singlet oxygen that results in a cascade of events such as endothelial cell membrane peroxidation, platelet aggregation and formation of a thrombi. This model was introduced by Rosenblum and El-Sabban in 1977 and later improved by Watson in 1985 in rat brains. This technique produces a localized infarct of desired size with well-delimited boundaries which makes it advantageous for precise cell characterization or functional studies in mice (Labat-gest and Tomasi, 2013). The photothrombosis technique shares similar mechanisms of stroke damage that occur in humans such as platelet aggregation and clot formation that interrupt blood supply in the area exposed to light (Dietrich et al., 1987).

Hydrogel as a drug delivery vehicle

Hydrogels are composed of a large amount of water (70 to 99%) and a cross-linked polymeric network. Hydrogels contain hyaluronan, commonly found in the extracellular matrix and therefore provide excellent biocompatibility. In situ-gelling hydrogels are injected in the liquid form and once inside the body transition into a sol-gel state. This causes the hydrogels to take the shape of the available space at the injection site. The ideal kinetics of hydrogel formation should initially be slow to prevent needle clotting, but fast enough to avoid dilution of hydrogel with the body fluids (Li and Mooney, 2016).

Research significance

During the initial phase of excitotoxicity, neurons are permanently damaged, and the associated brain function ceases rapidly. This phase is immediately followed by the recovery phase where the region adjacent to stroke damage (the peri-infarct zone) undergoes remapping and reorganization. However, this recovery is often not complete, making ischemic stroke a chronic disabling disease. The challenge for promoting recovery is to enhance neuroplasticity at the existing neuronal connections in the peri-infarct tissue.

Molecular mechanisms that underlie ischemic stroke recovery are identical to those involved in neuronal development. This critical period that displays heightened neuroplasticity that occurs during developmental stages also exists after stroke. Thus, studies have demonstrated that increasing cortical excitability in the peri-infarct zone 3 to 5 days after stroke improves outcomes in mice. Here, we show that administration of PbTx-2 epi-cortically 5 days after stroke enhances neural plasticity by increasing dendritic arborization and excitatory synapse density in the peri-infarct region and subsequently rescues motor deficits.

Hypothesis

We hypothesized that epicortical application of PbTx-2 in YFP expressing 2 to 4-month mice will lead to increased neuronal plasticity after photothrombotic stroke and will be accompanied by increased functional recovery when compared to vehicle-treated mice.

Objectives

The objectives of this study are to:

1) Evaluate neuroplasticity in PbTx-2 treated mice and compare with vehicle alone (by measuring dendritic arbor complexity, as well as immunohistological examination of excitatory synapse density levels)
2) Investigate the effects of PbTx-2 on motor recovery (by use of catwalk gait analysis, pasta matrix reach task and foot fault test).
3) Measure tritium-labelled PbTx-3 distribution in the mouse brain following epicortical administration by autoradiography.

Overview of experimental plan

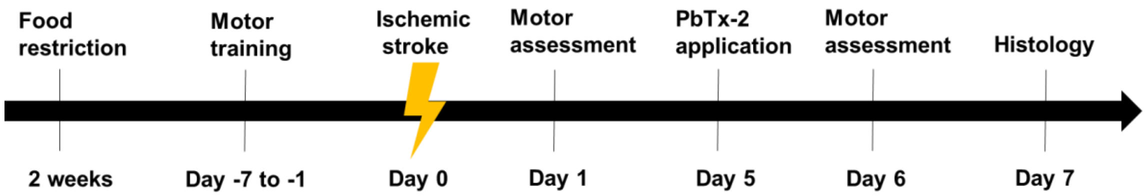

Figure 6 - Experimental timeline.

Animals were food restricted to 85% of their body weight for two weeks prior to training for pasta matrix reach task. Animals were trained to perform pasta matrix reach task and foot fault task prior to inducing stroke to obtain baseline values. A focal lesion was induced on the motor cortex region by photothrombosis on day 0. Animals were randomly divided into PbTx-2 treatment groups and vehicle-treated groups. On day 5, PbTx-2 groups were treated with 3, 10, 100, 1,000 or 3,000 pmol PbTx-2, whereas vehicle-treated mice were given hydrogel (vehicle) alone. Further, on day 1 (post-stroke) and day 6 (post-treatment) mice were assessed for the number of pasta pieces retrieved and % foot faults. On day 6, animals were sacrificed, and brains were isolated for histological analysis of surviving neurons in the peri-infarct region (Fig. 6).

CHAPTER 2: EFFECT OF PbTx-2 ON STRUCTURAL PLASTICITY POST-STROKE

Introduction

Pyramidal neurons

Pyramidal neurons comprise of 70-90% of all neurons in the cortex. Pyramidal cells form rich corticocortical connections, including both ipsi- and contralateral, as well as subcortical connections. Pyramidal neurons are primarily excitatory and are principal neurons of the cerebral cortex (Elston, 2007). Cortical pyramidal neurons are organized into six layers, each with characteristic dendrite branching patterns, associated with their functional roles (Spruston, 2008). Additionally, they are also found in subcortical structures such as the amygdala and hippocampus. These cells are characterized by their pyramidal shaped soma that range from 20- 120 μm in diameter and their prominent apical and basal dendrites (Fig. 7).

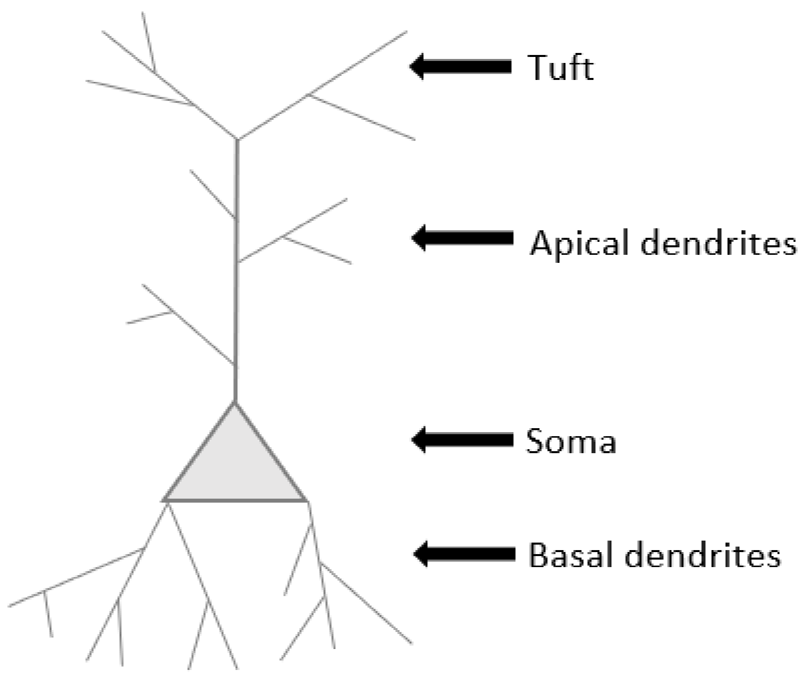

Figure 7 - Structural features of a pyramidal neuron

Dendrites and spines

During neuronal development pyramidal neurons elaborate their dendritic arbor complexity to increase their surface area and connectivity (Forest et al., 2018). Pyramidal neurons in the cortex have a characteristic pyramidal morphology with distinct large apical and shorter basilar dendrites that originate from the apex and base of the soma respectively. The pattern of dendritic arborization has a profound impact on the synaptic input field of the dendrite. Distinct dendritic regions integrate synaptic input from multiple sources (Spruston, 2008). In humans, dendritic structures are recognized approximately midway during gestation, spines appear later during the second trimester and reach peak at early infancy before the pruning that occurs during adolescence and adulthood (Forest et al., 2018). In rodents, once neurons mature, their arbors become relatively stable (Petit et al., 1988). However, there are exceptions to dendritic stability- for example, changes in basilar complexity have been noted in the cortex after brain damage (Biernaskie and Corbett, 2001; Jones and Schallert, 1992). Synapses are considered to be the major sites of information input in neurons. In the cortex, most of the excitatory synapses are formed on spines, whereas inhibitory synapses are usually formed on dendritic shafts and cell bodies. Dendritic spines are small protrusions that are studded along the dendritic shaft. Structurally, spines consist of a long thin neck and a mushroom shaped head that bears the excitatory synapse but can have varied morphology with different sizes and shapes (Bourne and Harris, 2008).

Vesicular Glutamate Transporter 1(VGLUT 1)

Vesicular glutamate transporters pack neurotransmitters inside synaptic vesicles and release them into the synapse. Three isoforms of glutamate transporters are expressed by glutamatergic neurons (VGLUT 1, -2, and -3). VGLUTs are dependent on a proton gradient that they create by hydrolyzing adenosine triphosphate (ATP). VGLUT1 and VGLUT2 are the two prominent isoforms in the adult brain. VGLUT1 also referred to as BNPI (brain-specific Na- dependent inorganic phosphate cotransporter) and SLC17A7 is predominantly expressed in the cerebellum, cortex and hippocampus, whereas VGLUT2 also referred to as DNPI (differentiation-associated Na-dependent inorganic phosphate cotransporter) and SLC17A6 is expressed in the brainstem, diencephalon, and spinal cord (Fremeau RT Jr, 2001).The third isoform, VGLUT3 also referred to as DFNA25 (deafness, autosomal dominant 25) and SLC17A8, is a nonconventional glutamatergic transporter as it is not expressed in glutamatergic neurons but is found in serotoninergic, cholinergic, and GABAergic neurons. (Gras et al., 2002; Fremeau et al., 2002)

Post-synaptic density (PSD-95)

Neurotransmitter receptors are known to be localized in the post-synaptic density (PSD) which is a protein rich subdomain that lines the inner surface of the postsynaptic membrane. The enrichment of receptors at PSDs occurs due to receptor immobilization by associated proteins in the postsynaptic membrane (Triller et al., 1985). PSD-95 is a membrane-associated guanylate kinase that plays a major role in regulating synaptic strength and assembling signaling complexes at excitatory synapses. The regulation of

PSD-95 is crucial for neurons establishing and maintaining proper synaptic connections (Matus, 2000)

Yellow fluorescent protein (YFP) transgenic mice

Mice express YFP under the control of neuron-specific elements from the thy1 gene. Thy1 is a member of the immunoglobulin superfamily that is expressed by neurons in many parts of the nervous system YFP fluorescence intensely stains in both live and paraformaldehyde-fixed tissue, allowing reexamination of tissue following live imaging. YFP labelling was confined to the neurons in their entirety, including somata, nuclei, axons, dendrites and spines and is the expression of thy1-YFP- H is restricted to neurons in layer V of the cortex (Feng et al., 2000).

Surgical procedures

Animals

All animal use protocols were approved by the Institutional Animal Care and Use Committee of Creighton University and employed measures to minimize pain and discomfort. Hemizygous Cg-Tg (B6.Cg-Tg(Thy1-YFP)HJrs/J (YFP expressing mice) were obtained from Jackson Laboratories (stock 3782) and maintained as a breeding colony. Mice were genotyped by a commercial vendor (Transnetyx, Cordova, TN). Murine *thy1*-YFP line-H strain was selected since they display bright fluorescence in layer V pyramidal neurons of the motor cortex providing high contrast, thus facilitating imaging and analysis of fine neuronal structures. (Feng et al., 2000.) Six days post infarct, animals were anesthetized and transcardially perfused with phosphate-buffered saline (PBS), followed by 4% paraformaldehyde (PFA) solution and tissue was isolated for analysis and post fixed overnight with PFA at 4 °C.

Photothrombotic model of focal stroke

Photothrombosis is less invasive and produces highly localized and reproducible lesions in comparison to other ischemic stroke models (Labat-gest and Tomasi, 2013). Adult *thy1*-YFP mice (Jackson Laboratories) age 2-4 months old were anesthetized with isoflurane inhalation (Piramal Healthcare; VetEquip) and placed in a stereotaxic apparatus (Stoelting). Body temperature was maintained at 36.9 ± 0.4°C using a TP700 water warming system (Stryker). A midline incision was performed, the skull exposed, and connective tissue removed. Mice were weighed and 100 mg/kg dose of Rose Bengal solution (10 mg/ml in sterile PBS) was injected intraperitoneally (IP). Five minutes after IP injection (Fig. 9), the brain was illuminated 1.5 mm lateral from bregma through an intact skull for 12.5 minutes using a light source (150 mW, KL 1500 LCD, Zeiss) attached to an UPlanApo20x objective (Olympus). Rose Bengal produces oxygen intermediates under light excitation, leading to platelet adhesion and aggregation, which occludes the vascular lumen and results in formation of an infarct. (Dietrich et al., 1987). The skull was closed using Vetbond adhesive (3M) and animals were treated for five days with oral Sulfamethoxazole and Trimethoprim (SMZ/TMP; 200/40 mg).

In vivo epicortical drug administration

Five days post-infarct (Fig. 8), adult *thy1*-YFP mice (Jackson Laboratories) age 2-4 months old were anesthetized with isofluorane inhalation (Kent Scientific; Vetflow) and placed in a stereotaxic apparatus (Stoelting). Body temperature was maintained at

36.9 ± 0.4°C using a TP700 water warming system (Stryker). The midline incision was reopened, and a small burr hole drilled (Dremel) through the skull 1.5 mm lateral to bregma. Hystem-HP Hydrogel alone or in combination with 3 pmol, 10 pmol, 100 pmol, 1,000 pmol or 3,000 pmol of PbTx-2 was injected using a Hamilton syringe 0.75 mm below the surface of the brain. PbTx-2 was dissolved in dimethyl sulfoxide (DMSO) (Sigma-Aldrich) and administered in a volume of 3 uL at a rate of 0.3 uL /min for an injection period of 10 min. The skull was closed using Vetbond adhesive (3M) and animals were treated for 1 day with SMZ/TMP.

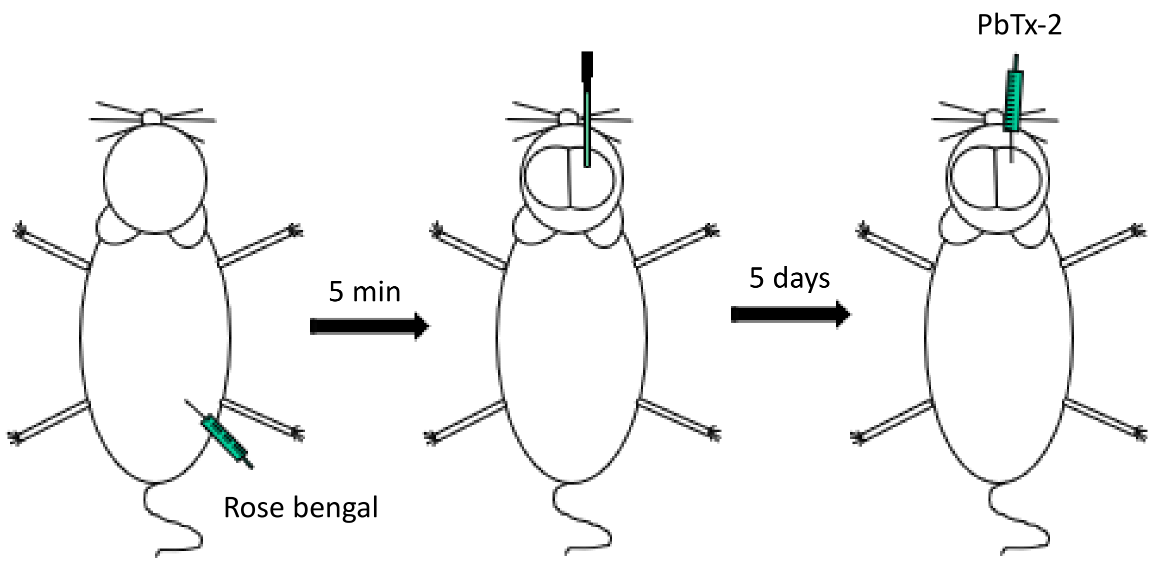

Figure 8 - Schematic model of photothrombotic stroke induction and PbTx-2 administration in mice.

Infarct volume

Infarct volume is commonly used to assess the extent of brain damage following an ischemic stroke event. We evaluated the effect of epicortical application of PbTx-2 on infarct volume determined by cresyl violet stain (Fig. 9). Cresyl violet is a basic dye that stains the acidic and basophilic components of Nissl bodies (granular endoplasmic reticulum), nucleoli of cells and chromatin in nuclei (Kobayashi and Lavenex, 2015). Coronal sections of 30 μm were cut using a vibratome (Leica VT 1200S). For infarct volume measurement, brain sections were stained by 0.5% cresyl violet (Nissl). Images were then acquired using bright-field microscope. The areas of infarct were delineated and quantified using the Image J software (NIH) and the infarct volume was calculated by summation of the lesion areas of all sections and integrated by the thickness of the section (Fig. 9B). Infarct volumes did not vary significantly between PbTx-2- and vehicle treated mice (Fig. 9C).

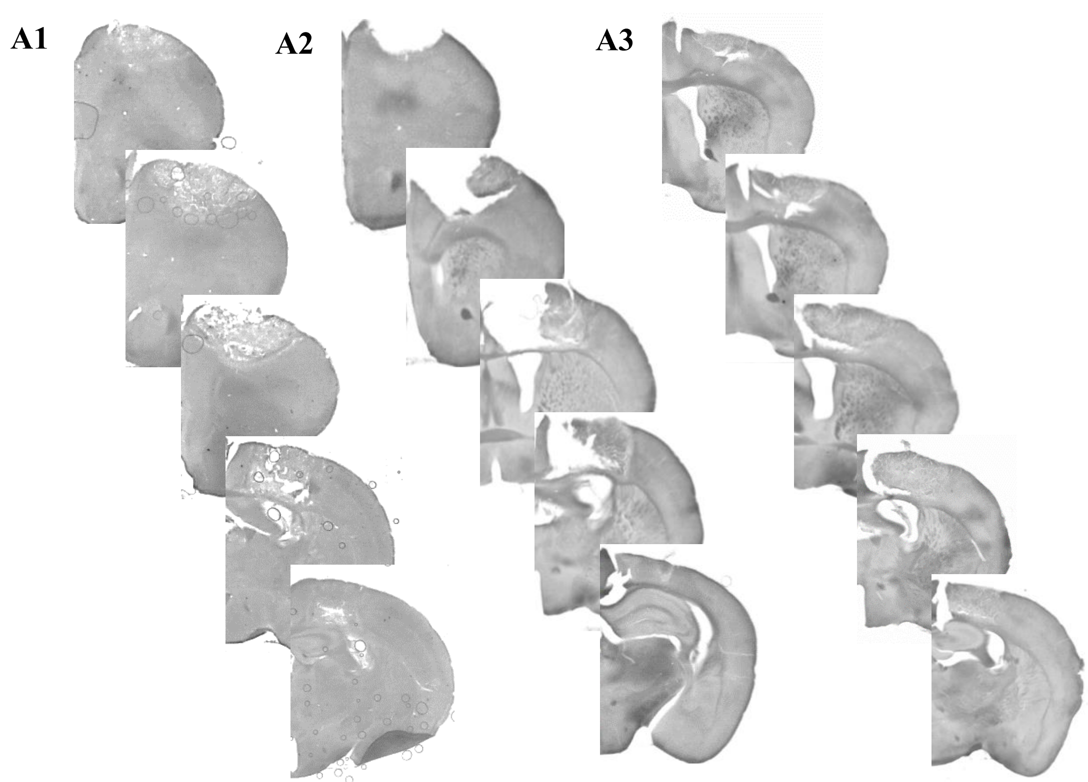

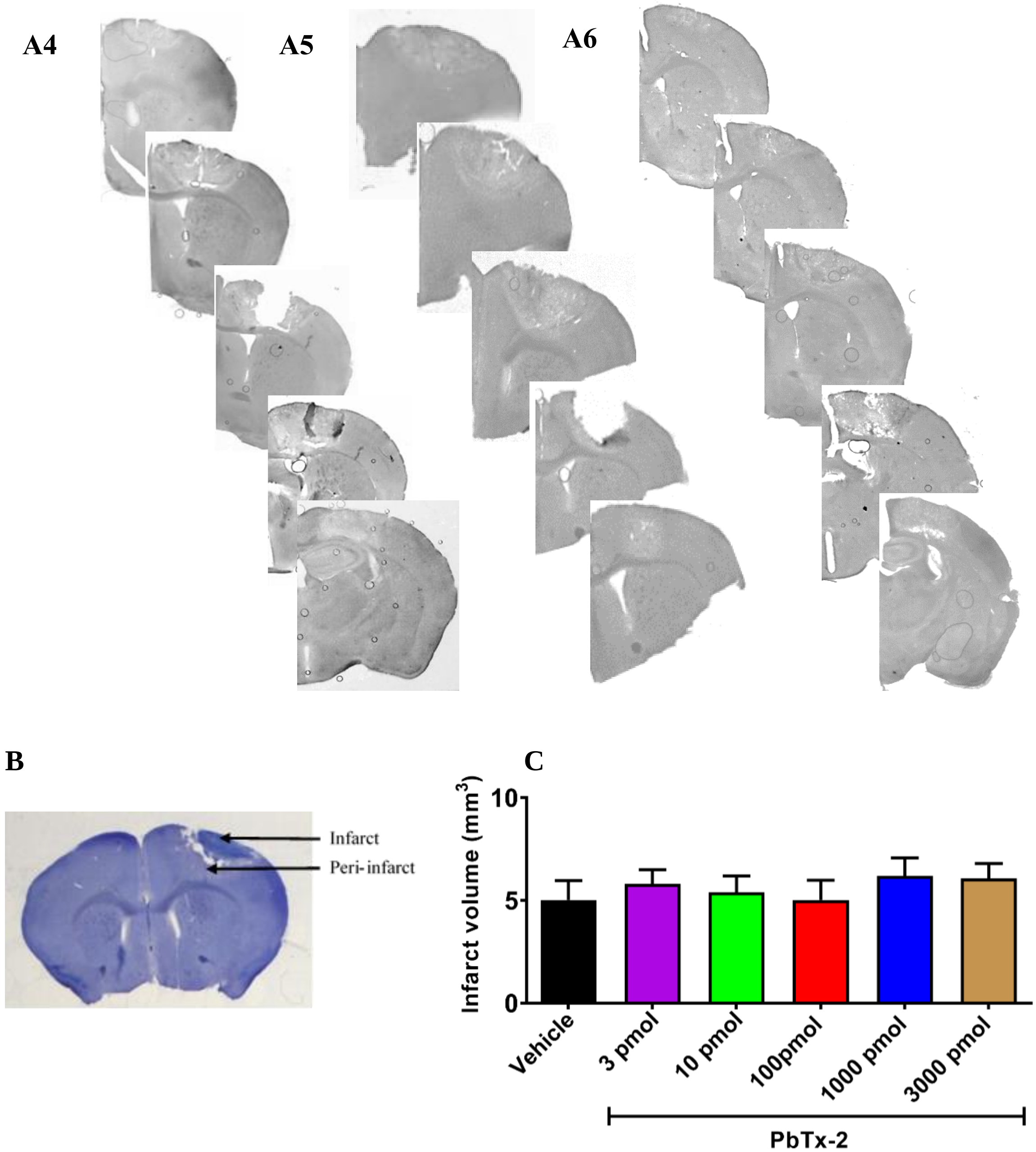
A4
A5
A6
B
Infarct
Peri-infarct
C
Infarct volume (mm^3)
10
5
0
Vehicle
3 pmol
10 pmol
100pmol
1000 pmol
3000 pmol
PbTx-2

Figure 9 – Photothrombotic stroke. Representative cresyl violet stained sections at 6-days post stroke from stroke + vehicle treatment (A1) and + stroke + 3, 10, 100, 1,000 and 3,000 pmol PbTx-2 treatment (A2, A3, A4, A5) respectively. (B) Zones of stroke indicating the photothrombotic stroke region and the peri-infarct region. (C) Quantification of stroke volume. No difference in stroke size, $p < 0.05$, one-way ANOVA. Data shown as mean ± SEM of 2 to 7 brains.

Apparatus

Leica SP8 Multiphoton Confocal Microscope

This system consists of an upright microscope, a smart touch panel, a smart control panel, and the computer system. Acquisition screen provides access to setting parameters such as resolution, scan speed, zoom, rotation, optical thickness and z-stack parameters. Additionally, it provides access to laser and detector settings associated with wavelength of the fluorochrome. The display screen displays the collected images (Fig. 10).

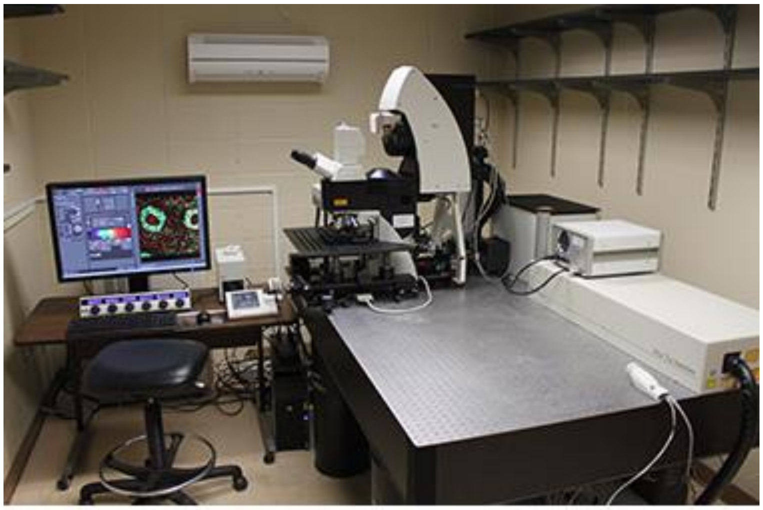

Figure 10 - Leica SP8 Multiphoton Confocal Microscope

Dendritic arbor complexity

Methods

100 μm brain sections were collected using a vibratome (Leica VT 1200). At least 10 neurons per animal were used for quantification. 40X images of YFP labelled layer V pyramidal neurons in the peri-infarct region were captured using a TCS SP2 confocal microscope in z-stack images (Leica Microsystems, Wetzlar, Germany). Each neuron selected for analysis met the following two criteria:

(1) the neuron was located in the peri-infarct region;(2) the neuron was distinctly separated from its surrounding neurons to allow measurement of dendritic arborization.

Following image acquisition, computer-based cell tracing software Imaris image analysis (Bitplane, Zurich, Switzerland) was used for 3D reconstruction of neurons (Fig 11 A). For the analysis of dendritic arbor complexity, dendritic tracings were quantified by the Sholl analysis method, where a set of concentric spheres (1μm apart) centered from the cell body was drawn, and the number of dendritic branch intersections at each sphere was quantified and plotted (Fig. 11 B).

A

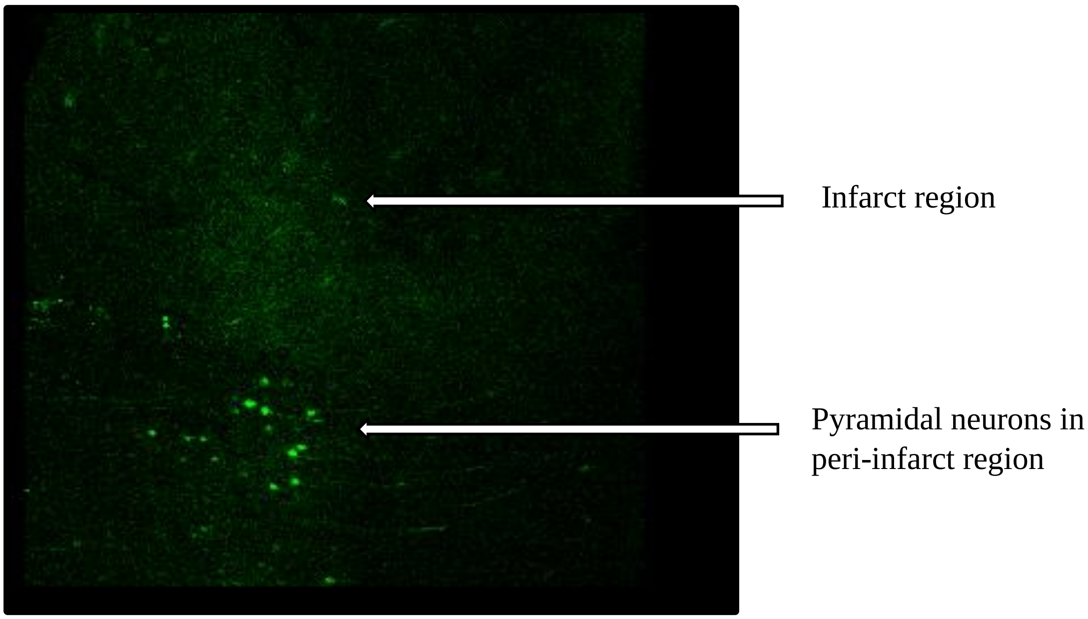

B

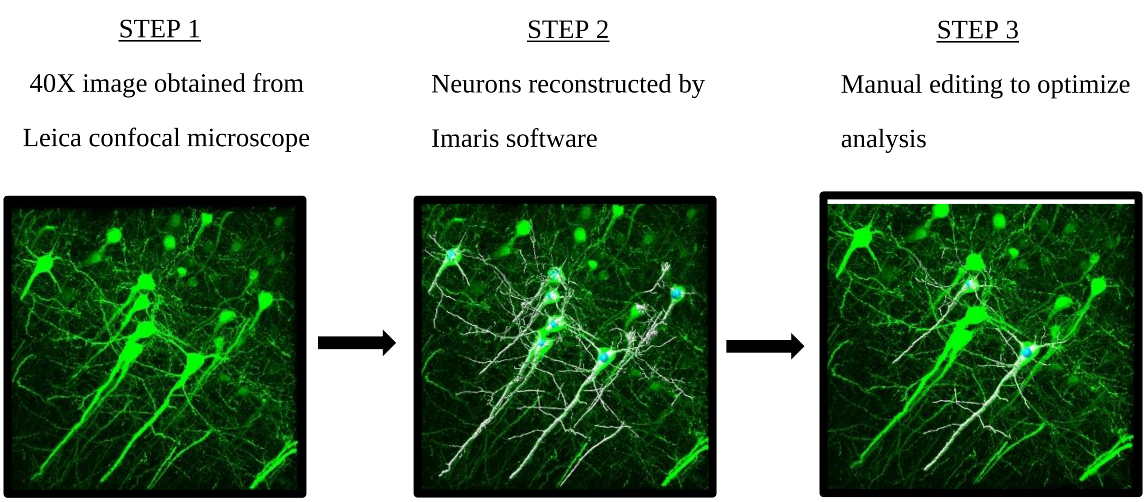

Figure 11 - Imaris image analysis. (A) 10 X image showing the infarct and peri-infarct region. (B) Steps involved in 3D reconstruction of dendrites using Imaris software

Results

A

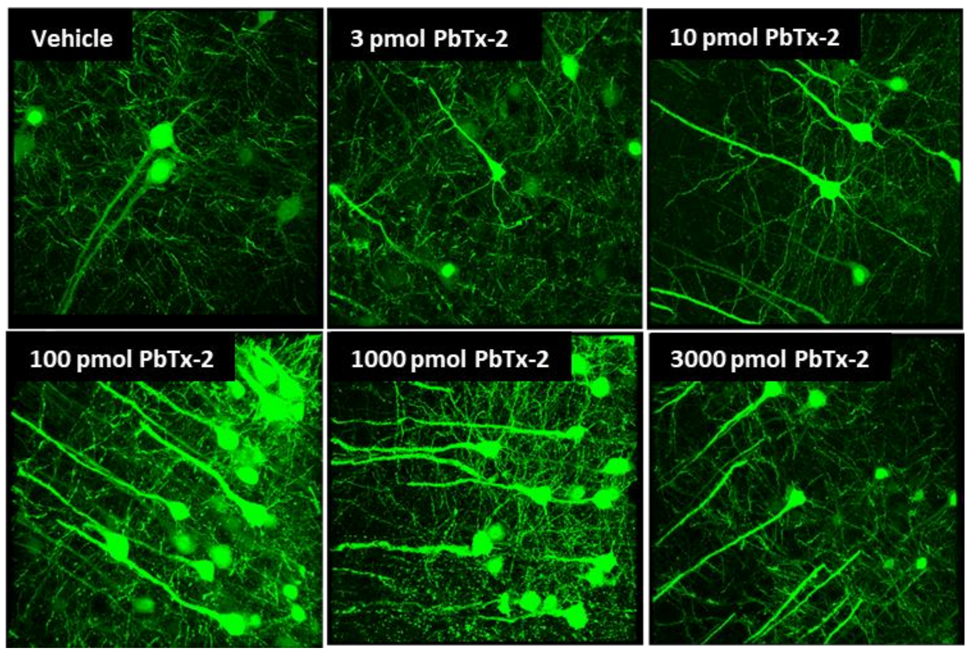

Vehicle
3 pmol PbTx-2
10 pmol PbTx-2
100 pmol PbTx-2
1000 pmol PbTx-2
3000 pmol PbTx-2

B

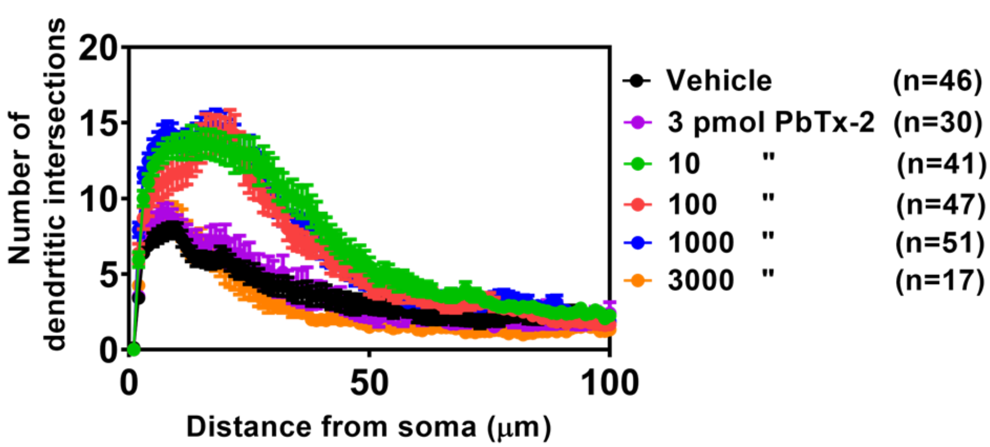

Number of dendrtitic intersections
20
15
10
5
0
0
50
100
Distance from soma (μm)
Vehicle (n=46)
3 pmol PbTx-2 (n=30)
10 " (n=41)
100 " (n=47)
1000 " (n=51)
3000 " (n=17)

C

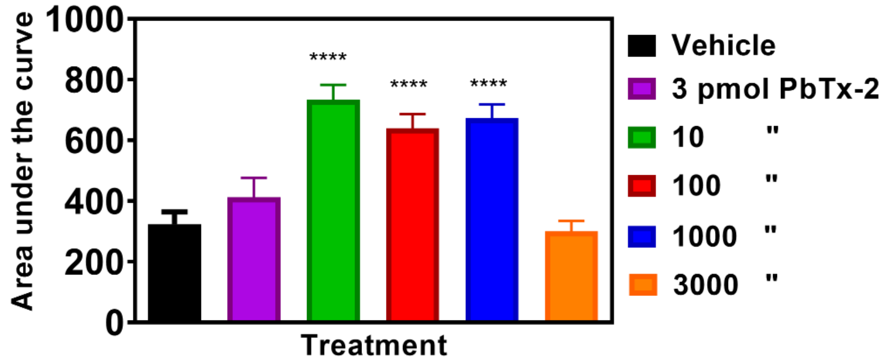

Figure 12 - Effect of PbTx-2 on dendritic arborization in the peri-infarct region. (A) Representative images of PbTx-2 induced dendritic arborization in the peri-infarct region (Scale bar: 30 µm) (B) Sholl analysis to quantify dendritic arbor complexity (C) Area under the curve (AUC) analysis of Sholl data. PbTx-2 at 10, 100 and 1,000 pmol doses enhanced dendritic arbor complexity in the peri-infarct site as compared to vehicle-treated animals (one-way ANOVA followed by Dunnett's post hoc test, ****$p<0.0001$). However, 3 and 3,000 pmol PbTx-2 treated mice lacked effects on expansion of dendritic arbors (3 pmol PbTx-2 effect, $p= 0.579$; 3000 pmol PbTx-2 effect, $p= 0.998$). Each bar represents the mean ± SEM of 17-51 neurons.

Dendritic injury is a pathological hallmark of excitotoxicity as NMDARs are predominantly localized on dendrites (Racca et al., 2000; Ikegaya et al., 2001). Six days post-infarct, confocal images of layer V YFP labelled pyramidal neurons were obtained and 3D morphological analysis of the arbor complexity with a defined algorithm was performed using Imaris image analysis software (Fig. 12 A). In vehicle-treated neurons, there is a gradual increase in branching complexity moving away from the soma reaching a maximum of 8 ± 0.5 intersections per neuron and then progressively declining beginning ~10 µm from the soma (Fig. 12 B). Dose- response analysis indicated that 10, 100 and 1,000 pmol PbTx-2 produced a robust 2-fold increase in expansion of dendritic arbors and a rightward shift in the Sholl plot as compared to controls. An AUC analysis of these Sholl data showed a significant increase in dendritic complexity following 10, 100 or 1,000 pmol PbTx-2 compared with vehicle-treated animals (Fig. 12 C). The PbTx-2 effect on dendritic complexity displayed a bidirectional profile, where there was a lack of effect on expansion of dendritic arbors in 3 and 3,000 pmol PbTx-2-treated mice.

Synapse density

Methods

Free-floating slices of 20 μm were washed three times in 0.1 M PBS and blocked in PBS buffer containing 10% goat serum in 0.25% Triton X-100 (Sigma-Aldrich) for 1 h. For synaptic staining, primary antibody solution was added consisting of PSD95 antibody (1:300, Invitrogen) and guinea pig polyclonal anti-VGLUT1 antibody (1:1000, EMD Millipore). Slices were incubated in primary antibodies overnight at 4°C, washed three times in 0.1 M PBS and 0.25% Triton X-100, and incubated with Alexa Fluor 594 goat anti-rabbit (1:500, Invitrogen), DyLight 405-conjugated AffiniPure Goat anti-guinea pig (1:500, Jackson ImmunoResearch). After incubation in secondary antibodies for 2 h, sections were washed and mounted onto slides using Fluoromount mounting medium (Sigma-Aldrich).

Images of immunostained brain sections were collected on Leica TCS SP2 confocal microscope using a 63x oil immersion objective in z-stack images. Serial optical sections at 0.15 μm intervals over a total depth of 10 μm for a total of 3 sections per brain were imaged. Channels for YFP, vesicular glutamate transporter 1 (VGLUT1) and postsynaptic density 95 (PSD-95) were acquired sequentially to prevent spectral overlap of fluorophores. Gain thresholds and amplitude offsets were kept constant between imaging of the ipsilateral and contralateral cortices. A ratio of synaptic puncta on the ipsilateral hemisphere to the contralateral hemisphere was obtained to eliminate within animal variations. Further, a spot detection algorithm in Imaris image analysis software was used to quantify synapse density (analysis was normalized to number of synapses per neurite length).

STEP 1: Collect 63 X images of dendrites in the peri-infarct region using a confocal microscope.

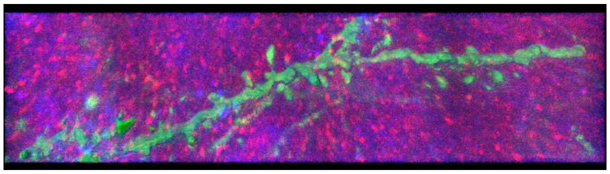

STEP 2: Using Imaris image analysis software, determine the surface of the dendrite.

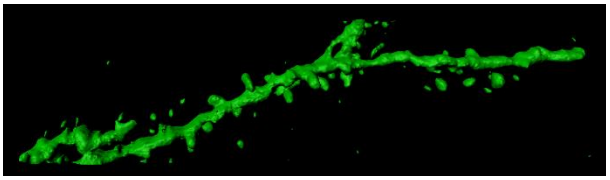

STEP 3: Using spot detection software algorithm, analyze colocalization of VGLUT1 and PSD-95 markers on the dendrite.

STEP 4: Normalize data by measuring length of the dendrite.

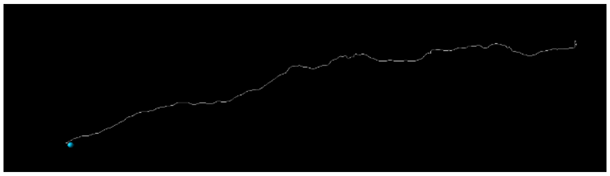

Results

A

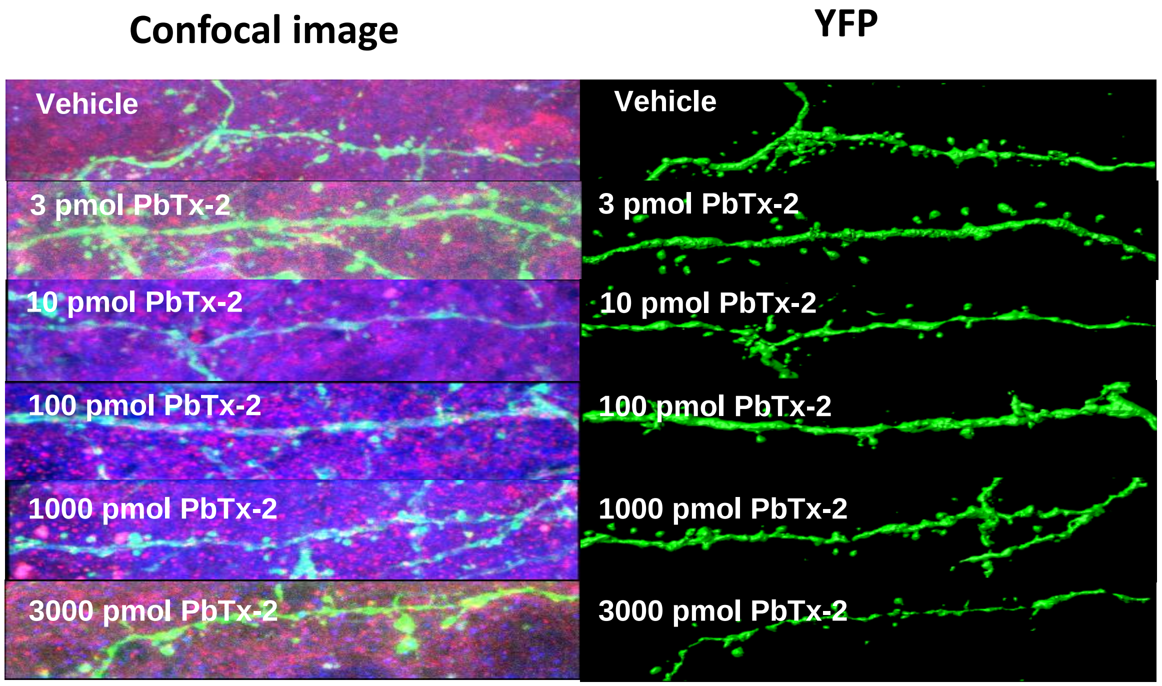

Confocal image
YFP
Vehicle
3 pmol PbTx-2
10 pmol PbTx-2
100 pmol PbTx-2
1000 pmol PbTx-2
3000 pmol PbTx-2

B

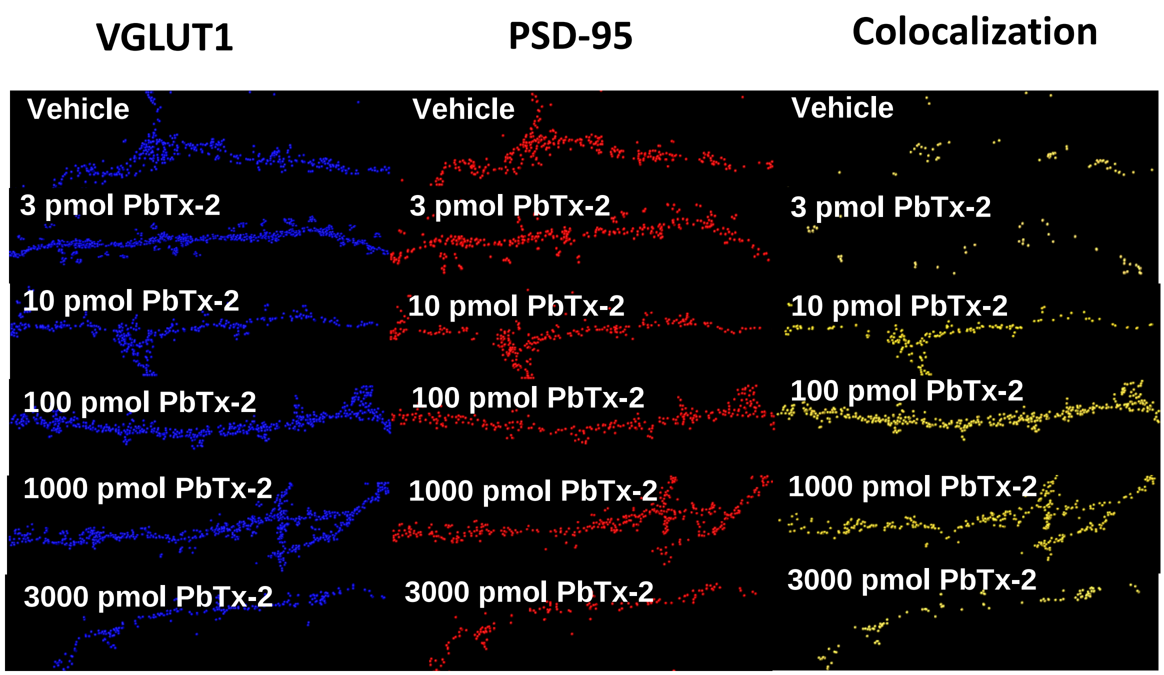

VGLUT1
PSD-95
Colocalization
Vehicle
3 pmol PbTx-2
10 pmol PbTx-2
100 pmol PbTx-2
1000 pmol PbTx-2
3000 pmol PbTx-2

C.

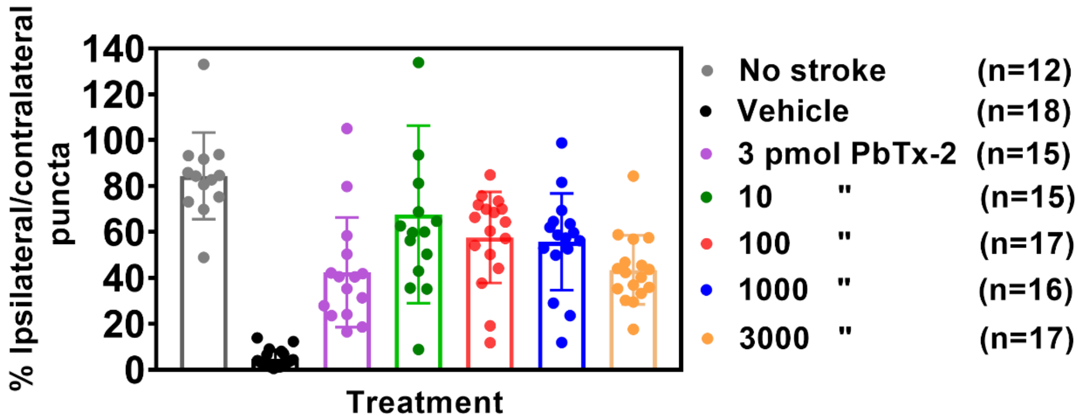

Figure 13 - Effect of PbTx-2 on excitatory synapse density in the peri-infarct region. (A) Representative images of double-immunostained YFP expressing neurites in the peri-infarct region at day 6 obtained from confocal microscope. (B) Antibodies against VGLUT1 (presynaptic marker/blue) and PSD-95/red (postsynaptic marker) were used to quantify synapse density, as indicated by colocalized fluorescent puncta (yellow) Scale bar: 5µm. (C) Quantification of colocalized fluorescent puncta using Imaris image analysis. We obtained the ratio of synaptic puncta on the ipsilesional side to that on the contralesional side to correct for within animal variation. 3, 10, 100, 1,000 and 3,000 pmol PbTx-2 doses enhanced synapse density in the peri-infarct region (one-way ANOVA followed by Dunnett's post hoc test, ****$p<0.0001$).

We examined the influence of PbTx-2 on synapse formation in the peri-infarct zone. Antibodies against VGLUT1 (presynaptic marker) and PSD-95 (postsynaptic marker) were used to quantify synapse density, as indicated by colocalized fluorescent puncta (Fig.13 A, B). Dose-response analysis of the effect of PbTx-2 on synapse density indicated that 3, 10, 100 and 1,000 and 3,000 pmol PbTx-2 produced significant increases in synapse formation (number of puncta per length of neurite) compared to control cortices (Fig.13 C). Further, we compared mean difference (MD) distribution between the PbTx-2 treated groups and controls using the Gardner-Altman mean comparison plot that affords transparency of the comparisons being made (Fig. 14 A, B).

Estimation statistics rather than hypothesis testing

The use of P values to define study results as significant or non-significant by relying on the 5% level of statistical significance provides little comparative information. Additionally, even precise P values fail to convey information of the size of the differences between study groups. In terms of sample size, small differences can be statistically significant with large sample sizes, but a study result may be statistically non-significant because of a small sample size. However, a confidence interval measures sample mean and mean difference between study groups to a range of values that are considered to be plausible for the sample population (Gardner and Altman, 1986). The width of the confidence interval is based on the standard deviation The difference axis provides more transparency of the comparisons being made. Importantly, by focusing attention on an effect size, the estimation plot encourages quantitative reasoning about the study (Ho J et al., 2019).

A

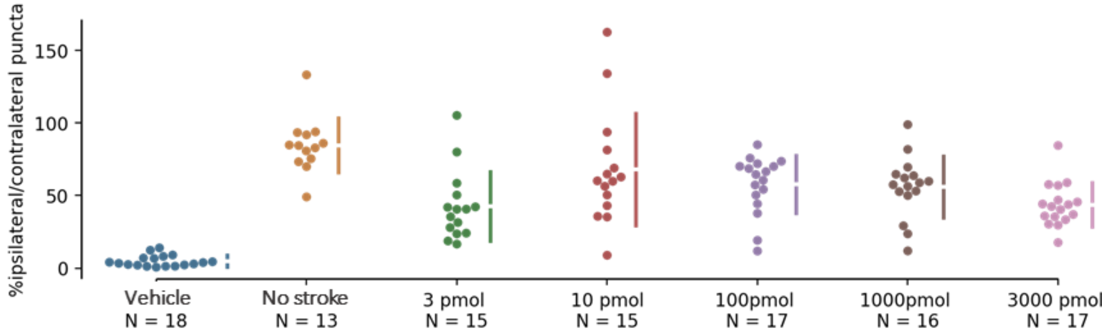

B

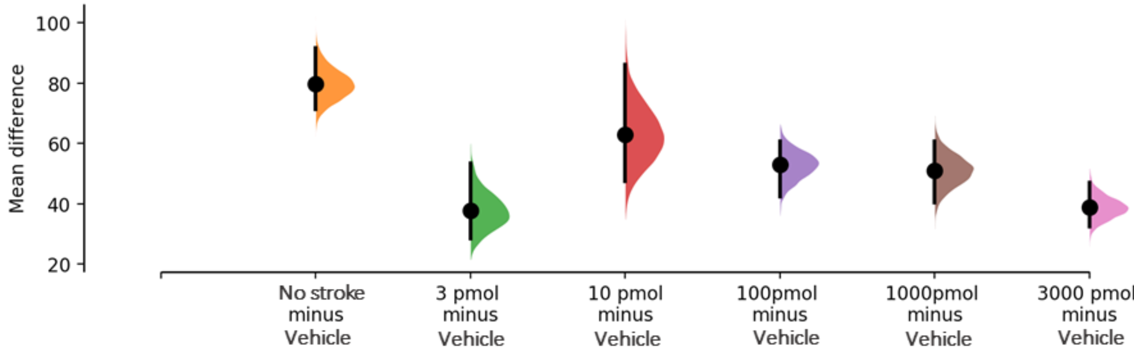

Figure 14- Gardner-Altman mean comparison plots. (A) Each plot contains comparisons for all PbTx-2-treated groups, and each dot represents % ipsilateral/contralateral puncta from an individual brain section. (B)The axis on the left side of the plot shows mean difference (MD) distribution between the PbTx-2-treated and vehicle-treated groups. 3 pmol PbTx-2 MD=37.6%, 95% CI [28.3, 53.4]; 10 pmol PbTx-2: MD= 63%, 95% CI [47.4, 86.2]; 100 pmol PbTx-2: MD=52.9%, 95% CI [42.3, 60.7]; 1,000 pmol PbTx-2: MD=51%, 95% CI [40.3, 60.6]; 3,000 pmol PbTx-2: MD=38.7%, 95% CI [32.4, 47.0]. The effect sizes and CIs are reported above as: effect size [CI width-

-lower bound, upper bound] and the narrowness of the confidence interval represents the effect size precision. All data represented as mean ± SEM of 12- 18 brain sections.

Data analysis

All data were presented as mean values ± SEM and plotted using GraphPad Prism® 7.0 (GraphPad, La Jolla, CA). Area under the curve (AUC) was used to assess the number of dendritic intersections for vehicle and PbTx-2 treatment groups. Gardner-Altman plot was generated using Estimation statistics software to compare mean differences between vehicle-treated and PbTx-2-treated groups. A one-way ANOVA followed by Dunnett's post hoc comparison test were used to compare 3 or more groups. The results were statistically significant if $p < 0.05$ according to the ANOVA. p values, the statistical analyses used, and sample sizes are described in the figure legends. Nonlinear regression (curve fit) was used to plot dose-response curves.

CHAPTER 3: EFFECT OF PBTX-2 ON MOTOR RECOVERY POST-STROKE

Introduction

Stroke is a common and a long-term cause of adult disability that is associated with severe motor deficits including partial paralysis (Rogers DC et al, 1997). Due to the devastating motor impairments caused by stroke with no current medical therapy, there is an urgent need for new pharmacotherapy. Mice serve as an excellent model to study human stroke and other brain injuries. In addition to examining the neuro histopathological changes, it is equally important to assess functional outcomes post-stroke. Identifying functional deficits and therapeutic treatments to restore function is essential for translational application to patients. Different tests are sensitive in detecting functional deficits associated with specific areas of brain damage. Table 3 provides an overview of the deficits each test identifies. To examine impairment and recovery, we utilized the CatWalk test to examine gross motor skills and gait, pasta matrix reach task to assess fine-motor skills (feeding and coordination) and the foot fault task to examine coordination and gait.

Functional test	Description
Rotarod test	Mice are placed on the rotating rod and try to remain on the rod to avoid falling. Latency to fall is quantified to evaluate motor function. This test is used to measure motor function and ataxia.

Pole test	Animals are placed on top of a pole and trained to turn around and descend the pole. Time taken to complete the task is measured to evaluate motor function.
Wire hanging test	Animals are suspended from a single wire stretched between two posts above the ground. Latency to fall is quantified to assess motor performance. This test measures grip strength, balance, and endurance.
Corner test	Animals are placed in two connected cardboard walls forming an angle with a small opening to motivate animals to enter deep into the corner. Once they walk into the corner their vibrissae will be stimulated causing them to turn to their left/ right side. This turning behavior is used to measure the impairment. This test detects sensory-motor asymmetry as mice typically turn to their ipsilateral side.
Adhesive removal test	A small adhesive patch is applied to each forepaw. The time to contact and removal of each adhesive tape is recorded. Animals typically remove the adhesive patch on their ipsilateral paw first.
Open field test	This test is used to evaluate motor function and exploratory behavior.
Gait analysis	Catwalk or DigiGait are video-based systems used to assess locomotor deficits of each paw while mice walk on a transparent surface.

Cylinder test	Animal is placed inside a glass cylinder; the forelimb use during the vertical exploration is measured by recording the number of forelimb contacts. This test is used to measure forelimb asymmetry post-stroke.
Pasta matrix reach task	Mice reach from a clear Plexiglass box through an aperture to retrieve pieces of pasta arranged in rows away from the aperture. This test is used to measure skilled forelimb movement.
Grip strength	Mice are trained to hold a grid that is attached to a force gauge. Following which they are gently pulled back from the base of the tail and the maximum force required before they let go is assessed.
Foot fault task	Animals are placed on an elevated grid and the number of foot faults made by the ipsilateral and contralateral limbs are counted during locomotion.
Ladder rung test	Animals walk across a horizontal ladder with irregularly spaced rungs. The number of foot slips during locomotion is assessed.

Table 3 - List of motor tests to assess stroke (Balkaya et al., 2013)

Catwalk gait analysis

Introduction

Noldus Catwalk XT and analysis system enables gait analysis in rodents by dynamic assessment of footfalls. CatWalk gait analysis has applications in detecting footfalls in several conditions such as spinal cord injury, muscular diseases, arthritis, neuropathic and inflammatory pain and Parkinson disease. CatWalk is a fully automated quantitative gait analysis system that uses a glass trackway and ventrally located camera to capture footfalls (Fig. 15). Compartments are created on either side of the trackway to contain the animal. Video recording of gait analysis is performed under dark room conditions. The footprints are captured at 100Hz with a high-speed color camera. Various gait metrics such as maximum contact, intensity, stride length is reported based on spatial and temporal data, and are labeled as per animal id/group

Default start and stop areas are used to automatically start and stop data acquisition. The start area is triggered as soon as an animal’s paw exceeds the values of pixel threshold in this area of the walkway. Similarly, data acquisition stops when the paws exceeding the threshold values disappear from the Stop area. In order to facilitate smooth runs between the Start and Stop area with a constant pace, the barrier (grill) and the start area have space between them so that when the animal is placed in the walkway next to the grill, it has some time to pick up pace before it enters the Start area. Space is also maintained between the Stop area and the grill on the other side of the walkway so that the animal does not slow down before it reaches the Stop area.

Figure 15-CatWalk gait analysis system.

After the classification of paws different gait metrics were calculated (Table 4).

Parameter	Definition
Intensity (%)	expressed as the mean brightness of all pixels of the print at Max contact
Maximum contact (%)	the time in seconds since the start of the data file at which the largest part of a paw contacts the glass plate
Stride length (%)	the distance (in pixels) between successive placements of the same paw (in pixels)
Stand (%)	The duration (seconds) of contact of a paw with the glass plate in a step cycle.
Swing (%)	The duration (seconds) of no contact with the glass plate in a step cycle.

Print length (%)	Length of the complete print. The complete print is the sum of all contacts with the glass plate as if the animal's paw would have been inked.

Table 4 - Definitions of gait parameters (CatWalk reference manual, Version 7.1, Noldus)

Methods

Training animals. Animals were trained to cross the walkway without interruptions so that all animals start from a similar baseline to compare runs and detect gait abnormalities. One week prior to the experiment, animals were trained to run across the walkway with a minimum of 3 crossings.

Data acquisition. This test was conducted in the dark to ensure optimal signal-to-noise ratio. Mice were required to walk on a glass plate, which was illuminated by a fluorescent light. Light enters at the long edge of the plate and is completely internally reflected and escapes only at those areas where the animal's paw makes a contact. A video camera, positioned underneath the glass plate, captures the illuminated areas and sends the video image to a computer running the CatWalk software (version 7.1, Noldus). Three runs per mouse were recorded before stroke and on days 1, 2 and 5 post-stroke and the average was used for analysis.

Footprint classification. (Fig. 16): After acquiring the video images of paw prints, labels were assigned to illuminated areas [right front (RF), right hind (RH), left front (LF), left hind (LH)]. Following footprint classification, the CatWalk software automatically calculates a wide number of parameters. A series of gait statistics were produced automatically when the system identified and marked each footprint. We then compared the ipsilateral LF paw to the contralateral RF paw in each animal of sham-operated (IP injection of PBS) and photothrombotic stroke (PTS) affected mice (IP injection of Rose Bengal).

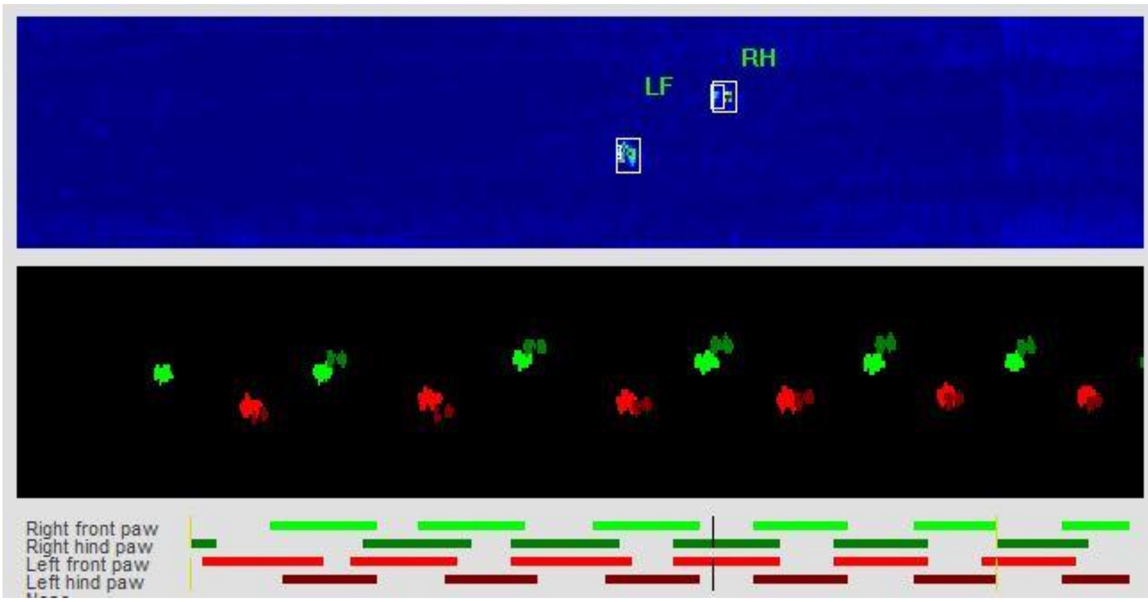

Figure 16-Footprint classification

Results

A

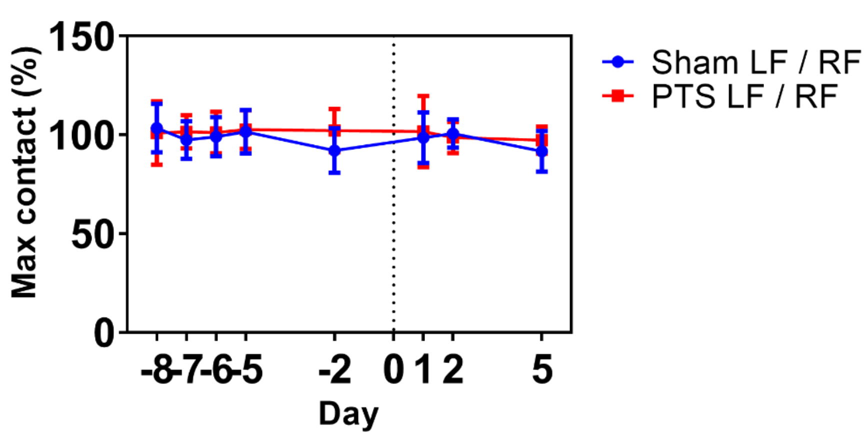

B

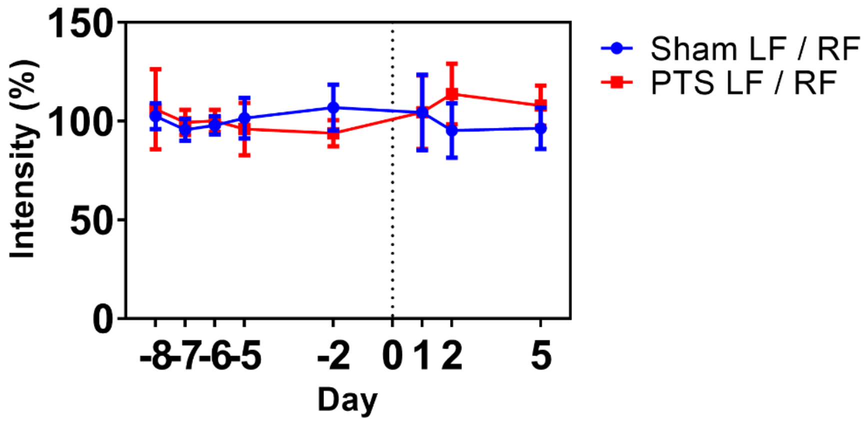
150
100
50
0
Intensity (%)
-8-7-6-5
-2
0
1
2
5
Day
Sham LF / RF
PTS LF / RF

C

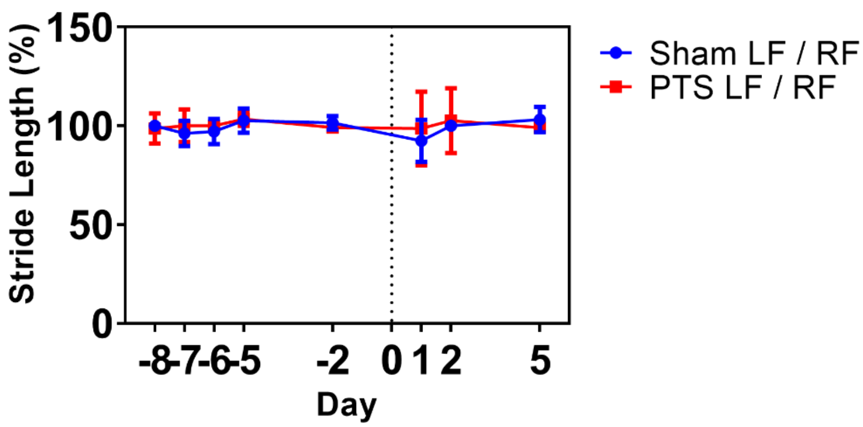
150
100
50
0
Stride Length (%)
-8-7-6-5
-2
0
1
2
5
Day
Sham LF / RF
PTS LF / RF

D

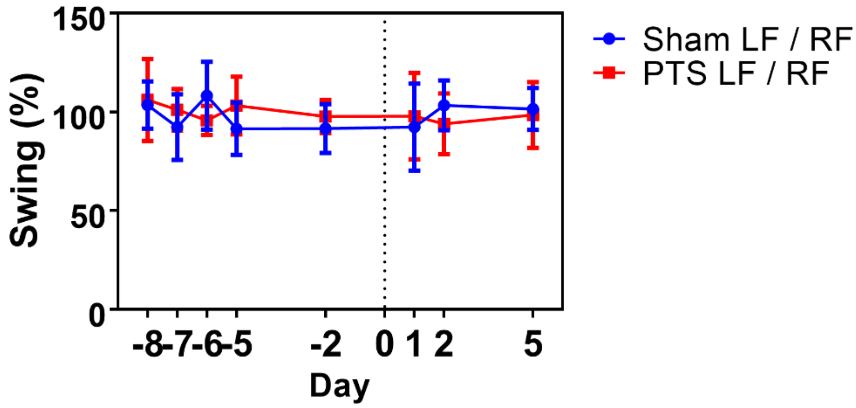
150
100
50
0
Swing (%)
-8-7-6-5
-2
0 1 2
5
Day
Sham LF / RF
PTS LF / RF

E

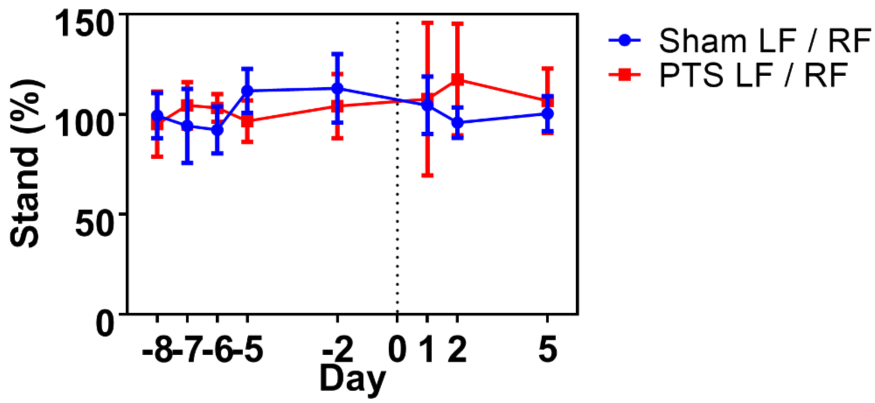
150
100
50
0
Stand (%)
-8-7-6-5
-2
0 1 2
5
Day
Sham LF / RF
PTS LF / RF

F

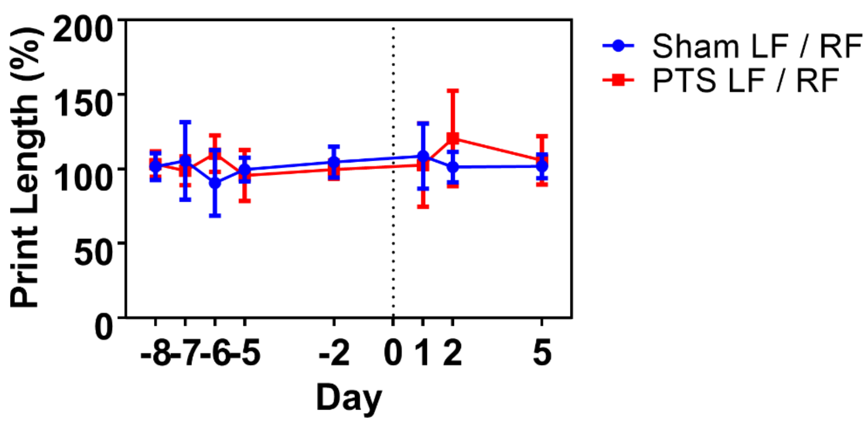
200
150
100
50
0
Print Length (%)
-8-7-6-5
-2
0 1 2
5
Day
Sham LF / RF
PTS LF / RF

Figure 17 - Impact of photothrombotic stroke on gross motor skills. Representative Catwalk parameters (A) max contact (%) (B) intensity (%) (C) stride length (%) analyzed before inducing photothrombotic stroke (PTS) to obtain baseline and on days 1, 2 and 5 after stroke. We compared ipsilateral left front (LF) paw to the contralateral right front (RF) paw. Gait parameters were not altered by photothrombotic stroke. $P < 0.05$ unpaired two-tailed test, values are given as mean ± SEM (n= 9 mice).

We evaluated if enhancing cortical excitability promoted gross motor gains after a focal stroke by performing CatWalk gait analysis. We specifically examined the contralateral forelimb as motor disability contralateral to the stroke affected hemisphere accounts for most dysfunctions (Mani et al., 2013). We analyzed several parameters on days 1, 2 and 5 post-stroke and compared the ipsilateral LF paw to the contralateral RF paw in each animal. No differences between the sham-operated group and PTS affected group were detected $p < 0.5$, n=9 mice; Fig. 17). Our results suggest that stroke induced motor deficits were confined specifically to the digits of the paw. This led us to perform pasta matrix reach task and foot fault test to assess fine motor skills as catwalk gait analysis only detected gross motor deficits.

Foot fault task

Introduction

The foot fault task, also referred to as the grid walking task, is commonly used to assess motor impairments of limbs during locomotion in rodents and requires minimum pre-training. This test is useful for assessing early treatment effects due to spontaneous recovery (Modo et al., 2010). This task has found applications to identify motor coordination deficits and rehabilitation effects post-stroke. Animals are placed on an elevated grid and are allowed to walk freely. Animals with no stroke will typically place their paws precisely on the grid while moving (Barth et al., 1990). Each time a paw slips through the grid openings a "foot fault" is recorded through a video camera. Stroke affected mice typically make significantly more contralateral foot faults than intact mice.

Methods

Each mouse was placed individually on the elevated wire grid and allowed to freely walk for a period of 5 min. Video footage was analyzed and the total number of foot faults for each limb, along with the total number of non-foot-fault steps, was counted, and a ratio between foot faults and total steps taken calculated (Fig. 18). Percent foot faults were calculated by: number of foot faults / (foot faults + number of non-foot-fault steps) × 100. A step was considered a foot fault if it was not providing support and when the foot went through the grid hole (Clarkson et al., 2010). To avoid variations, a ratio between foot faults and total steps taken was taken into account for differences in the degree of locomotion between animals and trials.

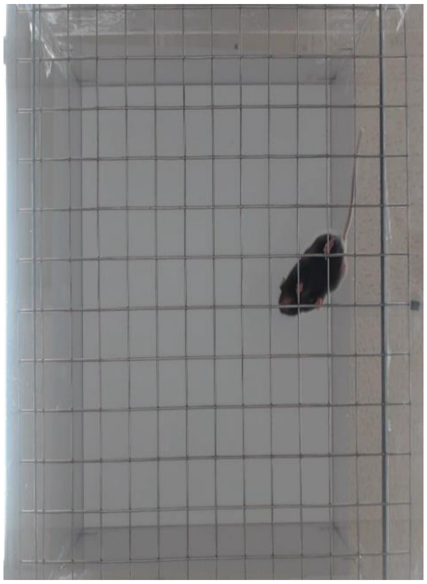

Figure 18 - Foot fault training

Results

A

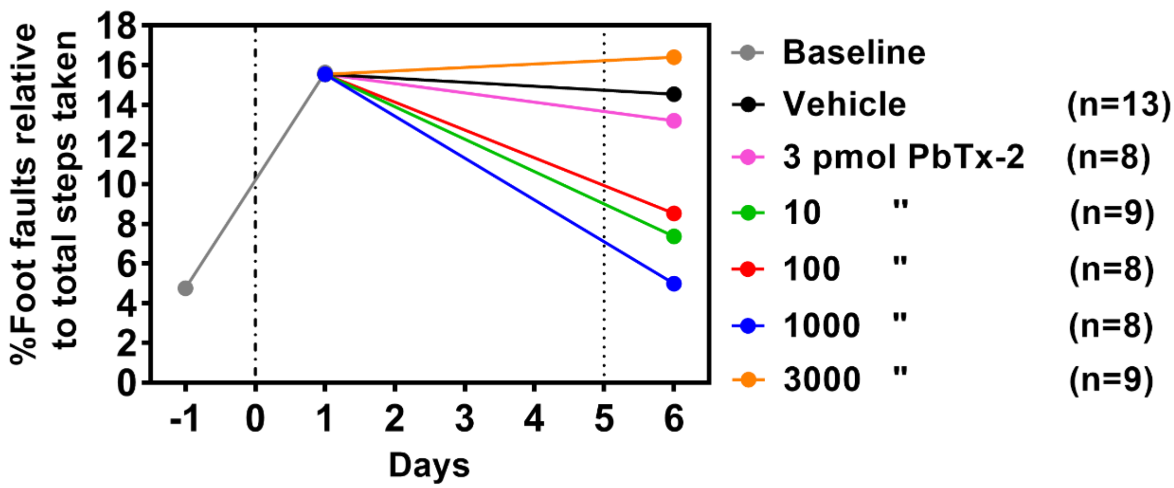

%Foot faults relative to total steps taken
18
16
14
12
10
8
6
4
2
0
-1
0
1
2
3
4
5
6
Days
Baseline
Vehicle (n=13)
3 pmol PbTx-2 (n=8)
10 " (n=9)
100 " (n=8)
1000 " (n=8)
3000 " (n=9)

B

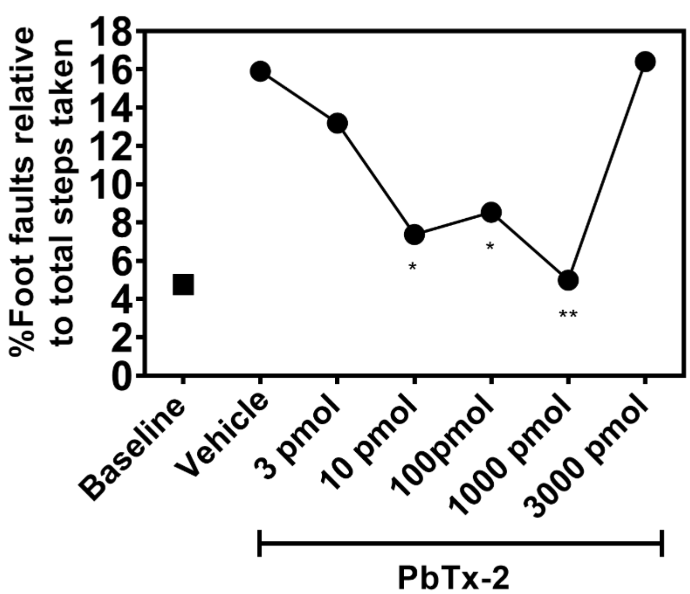

%Foot faults relative to total steps taken
18
16
14
12
10
8
6
4
2
0
*
*
**
Baseline
Vehicle
3 pmol
10 pmol
100pmol
1000 pmol
3000 pmol
PbTx-2

Figure 19 - Effect of PbTx-2 treatment on foot fault task. (A) Animals were trained to walk on an elevated grid prior to inducing stroke to obtain baseline values. (B) Quantification of PbTx-2 dose-response effects on motor recovery. 1 day after inducing stroke, a significant increase in % foot faults were observed. 10, 100 and 1,000 pmol PbTx-2-treated animals displayed significant improvement in % foot faults as compared to vehicle-treated animals (one-way ANOVA followed by Dunnett's post hoc test, 10 pmol PbTx-2 effect; *p=0.023, 100 pmol PbTx-2 effect; *p=0.027, 1000 pmol PbTx-2 effect; **p=0.001). Whereas, 3 and 3,000 pmol PbTx-2 did not aid recovery (3 pmol PbTx-2 effect, p=0.703; 3000 pmol PbTx-2 effect, p>0.999). All data are represented as mean ± SEM (n=9 to 13 mice).

The Foot Fault task is a sensitive indicator for detecting motor deficits of limb functioning and placement during locomotion. Animals with no stroke place their paws precisely on the wire frame and demonstrate few to no foot faults. (Schaar et al., 2010). Stroke produced a significant increase in the % foot fault 1 day after the insult, indicating a focal stroke was successfully induced (Fig. 19A). 10, 100 and 1,000 pmol PbTx-2-treated animals displayed a significant improvement in % foot faults as compared to vehicle-treated animals. Whereas, 3 and 3,000 pmol PbTx-2 again did not promote recovery (one-way ANOVA followed by Dunnett's post hoc test, 10 pmol PbTx-2 effect; *p=0.023, 100 pmol PbTx-2 effect; *p=0.027, 1000 pmol PbTx-2 effect; **p=0.001; 3 pmol PbTx-2 effect, p=0.703; 3000 pmol PbTx-2 effect, p>0.999; n= 9 to 13 mice; Fig. 19 B) These data suggest that treatment with 10, 100 and 1,000 pmol PbTx-2 on day 5 resulted in functional recovery of fine motor skills in foot fault task as compared to vehicle only.

Pasta matrix reach task

Introduction

This motor test allows for quantitative motor assessments of both motor impairment and recovery after stroke. Although this test requires food deprivation and daily pre-training to teach mice to retrieve pieces of pasta, the test is relatively easy to score.

Methods

To facilitate training, animals were food restricted for two weeks so that their body weight gradually reached 85% of that expected with free access to food. Animals were placed in a plexiglass cylinder and trained for 30 minutes to reach through a 1 cm wide slot to grasp, break, and retrieve pieces of vertically oriented pasta (Angel Hair Pasta, American Beauty) inserted into a 1mm diameter grid-ordered field of holes.

To initially encourage reaching and to determine paw preference, animals were trained to grab a single piece of pasta for 3 days (Fig. 20 A). Once the preferred paw was determined, the matrix was offset such that animals could retrieve pasta pieces only with their preferred paw. Additionally, the matrix was arranged such that it consisted of a 5X5 vertical alignment of 5 cm long segments of uncooked pasta (Fig. 20 B). Subsequent training sessions for a period of 7 days led to improved success in the task and established a baseline. Stroke was induced in the brain hemisphere contralateral to the preferred paw. Performance was quantified by manual inspection of the matrix at the end of the session (counting the number of broken pasta pieces).

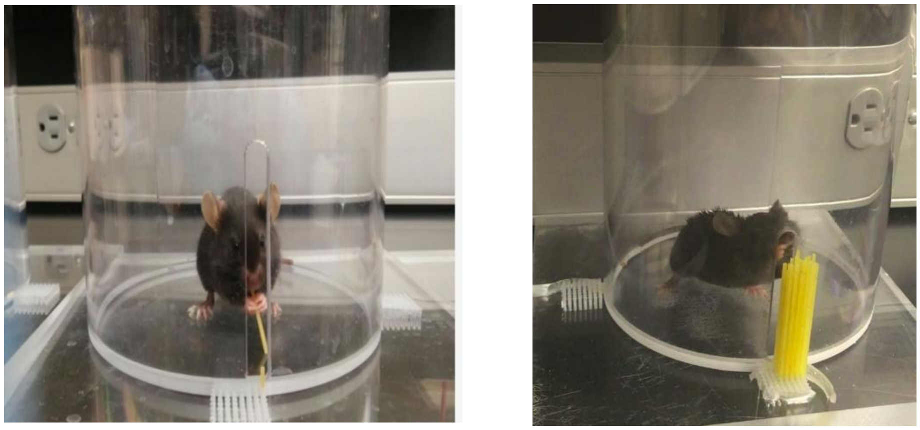

Figure 20 - (A) Paw preference training (B) Pasta matrix reach task training.

Results

A

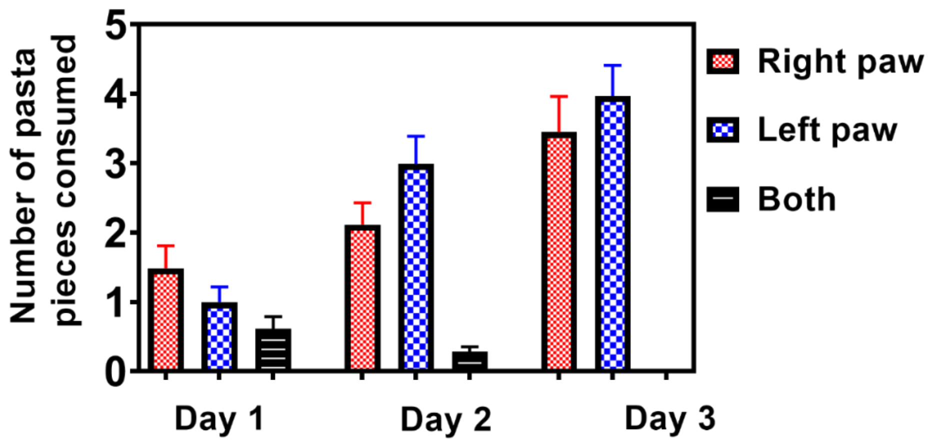

Number of pasta pieces consumed
5
4
3
2
1
0
Day 1
Day 2
Day 3
Right paw
Left paw
Both

B

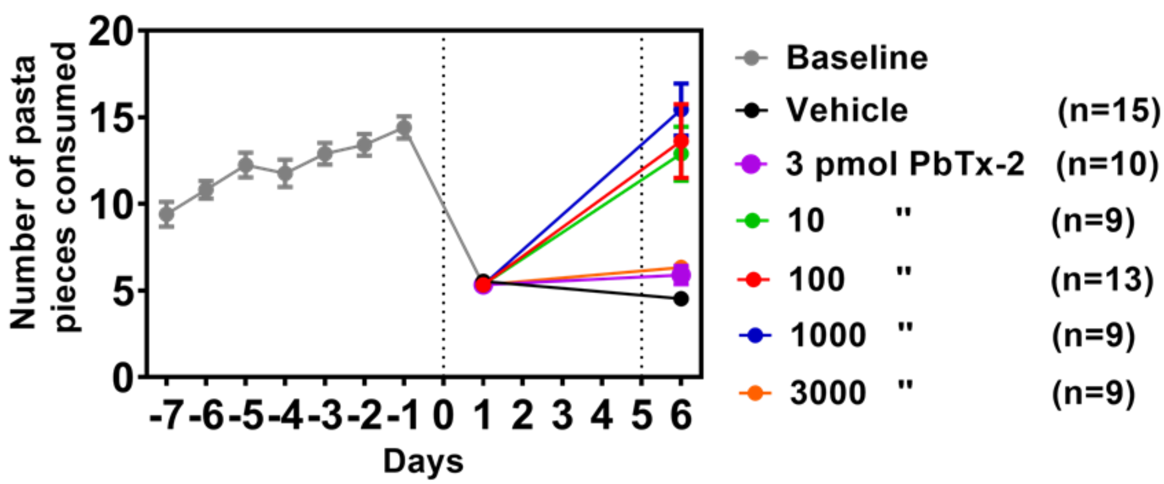

Number of pasta pieces consumed
20
15
10
5
0
-7 -6 -5 -4 -3 -2 -1 0 1 2 3 4 5 6
Days
Baseline
Vehicle (n=15)
3 pmol PbTx-2 (n=10)
10 " (n=9)
100 " (n=13)
1000 " (n=9)
3000 " (n=9)

C

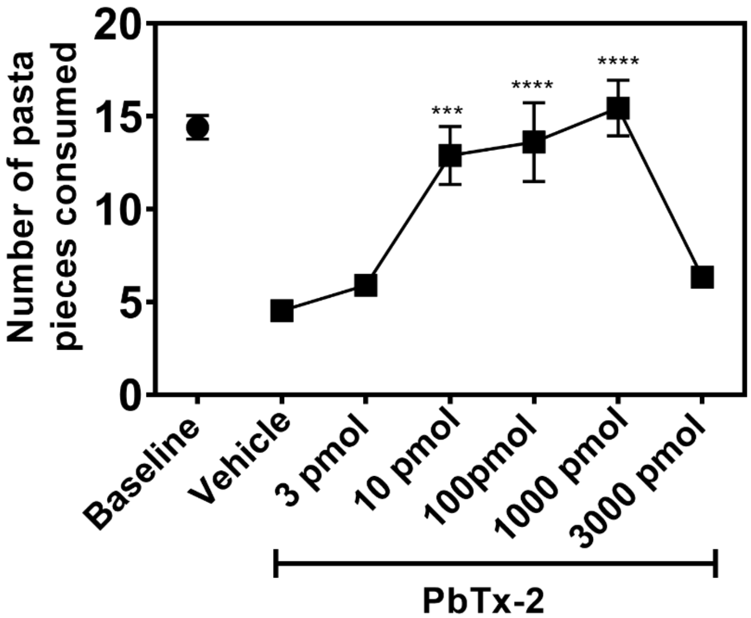

Figure 21 - Effect of PbTx-2 treatment on pasta matrix reach task. (A) Paw preference was determined using a single piece of pasta for 3 days (B) Animals were trained for 7 days to retrieve 25 pieces placed in a 5X5 matrix from their preferred paw to obtain baseline values. (C) Quantification of PbTx-2 dose-response effects on motor recovery. 1 day after the stroke, significant reduction in the number of pasta pieces retrieved indicating motor deficits induced by the insult. On day 6-10, 100 and 1,000 pmol PbTx-2-treated animals exhibited a significant increase in the number of pasta pieces retrieved as compared to vehicle-treated animals (one-way ANOVA followed by Dunnett's post hoc test, ****$p<0.0001$, ***$p=0.0002$). 3 and 3,000 pmol PbTx-2 did not facilitate functional recovery (3 pmol PbTx-2 effect, $p=0.955$; 3000 pmol PbTx-2 effect, $p=0.873$). All data are represented as mean ± SEM (n=9 to 15 mice).

Rodents live in an environment that requires use of a complex range of motor skills to gain access to food (Schallert et al., 2005). Pasta matrix reach task is one of the few motor tests that can measure skilled forepaw use (Schaar et al., 2010). Mice were trained for 3 days to grab a single piece of pasta to determine paw preference (Fig. 21 A).

Once the preferred paw was determined, mice were trained for 7 days to obtain baseline values before inducing stroke (Fig. 21B). On day 1, stroke produced a significant decline in the number of pasta pieces retrieved, indicating photothrombotic stroke affected fine motor skills. On day 6, animals treated with 10, 100 and 1,000 pmol PbTx-2 exhibited a significant increase in the number of pasta pieces retrieved as compared to vehicle-treated animals. 3 and 3,000 pmol PbTx-2 did not facilitate functional recovery (one-way ANOVA followed by Dunnett's post hoc test, ****$p<0.0001$, ***$p=0.0002$; 3 pmol PbTx-2 effect, $p=0.955$; 3000 pmol PbTx-2 effect, $p=0.873$; n= 9 to 15 mice; Fig. 21 C).

Data analysis

All data were presented as mean values ± SEM and plotted using GraphPad Prism® 7.0 (GraphPad, La Jolla, CA). The differences in gait assessed by CatWalk between sham-operated mice and stroke affected mice were examined using an unpaired t (two tailed) test. Percent foot faults were calculated by: number of foot faults / (foot faults + number of non-foot-fault steps) × 100. A one-way ANOVA followed by Dunnett's post hoc comparison test were used to compare 3 or more groups. The results were statistically significant if $p < 0.05$ according to the ANOVA. p values, the statistical analyses used, and sample sizes are described in the figure legends. Nonlinear regression (curve fit) was used to plot dose-response curves.

CHAPTER 4: DISTRIBUTION OF TRITIUM-LABELLED PBTX-3

Autoradiography

Introduction

Autoradiography is a detection method in which X-ray, or a photographic film is exposed to emissions from radio-labelled isotopes to produce an image as darkened spots on the film. After a time-dependent exposure, the film is developed to reveal the location of the areas of radioactivity which are identified as zones of varying optical density. The density is related to the amount of radioactivity in the zone. Quantification can be done either by densitometry using a calibration curve produced by exposure to radioactive standards or by removing the areas of radioactivity and counting them by liquid scintillation (Clark, 2000).

Apparatus specifications

X ray cassette. X ray cassette is a flat-light resistant container used to hold a film in close contact with the radioactive specimen.

High performance autoradiography film. A double-coated, multipurpose film with a clear base specially designed for the detection of beta- and gamma- emitting isotopes.

Developer. Konica SRX-101 A allows fast development of radiographs. It typically consists of a control panel to adjust setting and a 17-inch feed tray where a large radiograph or 2 small 8 x 10 films can be processed side to side in just 90 seconds per cycle.

Methods

In order to study the distribution of PbTx-2, an epicortical application of tritium (^{3}H) labeled PbTx-3 was performed in photothrombotic stroke induced mice. Animals were sacrificed at different time points such as 5, 15, 30 minutes and 2 hours after administration and their brains were rapidly removed and frozen over dry ice. The frozen brains were then mounted on the cryostat chuck. Serial sections of 30 µm were then taken coronally on a cryostat (Leica CM 1900) maintained at 20°C. Sections were then mounted onto slides and placed inside X-ray cassettes. Autoradiograms were then generated by apposition of slide-mounted sections to ^{3}H-sensitive Amersham Hyperfilm MP (GE Healthcare) for 6 weeks (Fig. 22 A). The images were then developed using Konica Medical Film Processor SRX-101.

Results

To quantify the extent of distribution of tritiated PbTx-3, microdensitometric analysis was performed using 1619 x 762 µm samples taken from the region of maximum optical density for a series of autoradiograms generated from coronal sections taken to encompass the complete stroke region (Fig. 22 A). By plotting the optical density for each section from the point of injection to a level not different from background, PbTx-3 at 5, 15 and 30 minutes reached approximately 600 µm from its injection site. (Fig. 22 B).

A

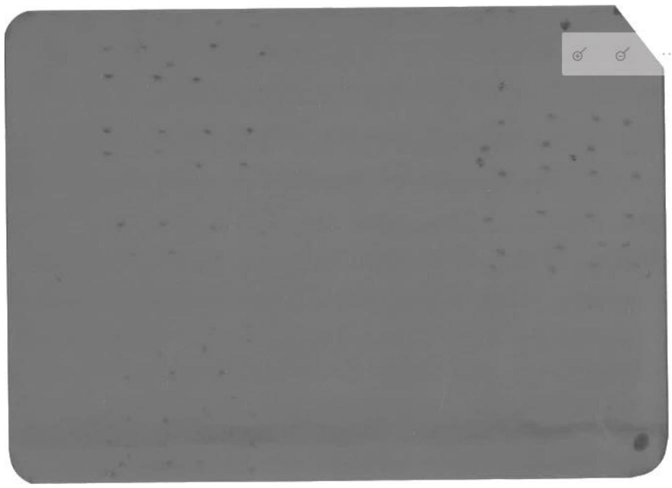

B

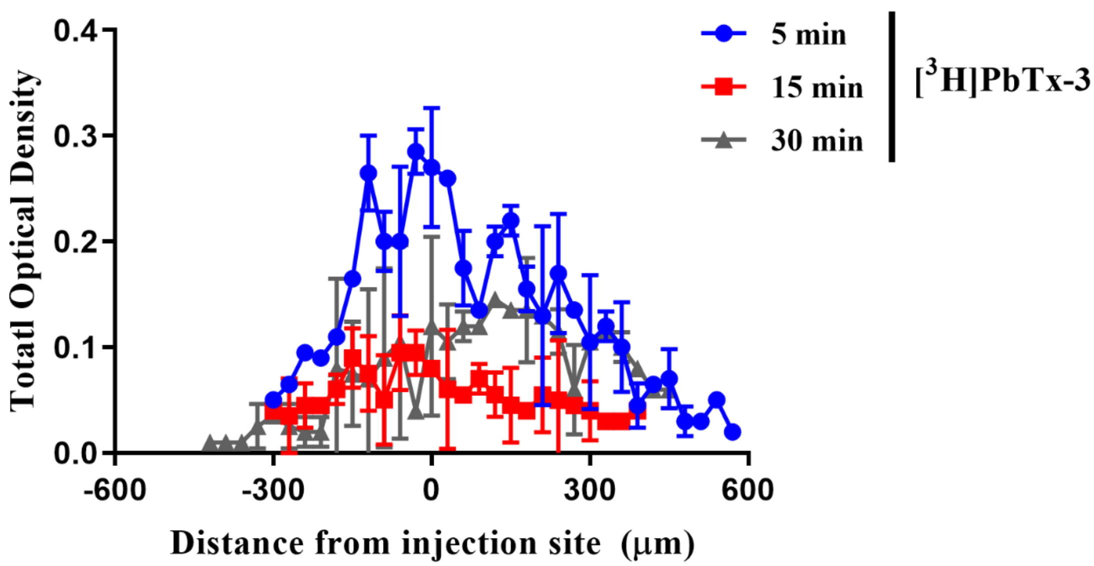

Figure 22 – Distribution of [^{3}H] PbTx-3 in the brain. (A) Representative film processed 6 weeks after exposure to [^{3}H] labelled PbTx-3 treated brains (B) Autoradiographic analysis of [^{3}H] PbTx-3 5, 15, 30 min after an epicortical application onto the stroke site.

Discussion

Here, we investigated the effect of PbTx-2 on neuroplasticity in the peri-infarct cortex and associated motor functions in a murine model of stroke. The main findings of this study are:

1. Epicortical application of PbTx-2 in the stroke site displayed a 2-fold increase in dendritic arborization and increased synaptogenesis at the peri-infarct site.

2. Photothrombotic stroke model produced functional deficits that was confined to the digits of the paw as no significant gross motor deficits were observed in CatWalk gait analysis.

3. Results of cortical plasticity also correlated to a dramatic improvement in the functional outcome as measured by an increase in the number of pasta pieces retrieved and decreased % foot faults.

VGSCs play a fundamental role in electrical signaling of the nervous system and for action potential generation (Hille B, 2001). Two-photon imaging studies show that synaptic stimulation leads to transient increases in $[Na^+]_i$ in postsynaptic spines and dendrites (Rose et al., 1999). Thus, indicating that $[Na^+]_i$ is a major signaling molecule and plays a role in activity-dependent synaptic plasticity. PbTx-2, a VGSC modifier, augments NMDA receptor signaling by coincidence of an elevation of $[Na^+]_i$ and Src kinase (Dravid SM et al., 2005). Previous reports (George et al., 2012) suggested that PbTx-2 mediated activation of sodium channels with attendant enhancement of NMDA-induced Ca^{2+} influx accelerated spine formation and maturation, dendritic arbor elaboration and synaptogenesis in developing cerebrocortical neurons. On a molecular level, increased Ca2+ evoked by PbTx-2 produced phosphorylation of Ca2+-dependent molecules, such as CaMKI, CaMKII and CREB that play an essential role in neuronal growth and survival. BDNF is an activity-dependent neurotrophic factor that mediates neuroplasticity and is regulated by CREB -dependent mechanisms (Tao X et al., 1998) Further, PbTx-2 exposure also increased the surface expression of BDNF-tropomyosin-related kinase B receptors in cerebrocortical neurons.

Glutamate plays an essential role in mediating excitatory neurotransmission in the central nervous system and is vital for synaptic plasticity. After an ischemic stroke, however, glutamate accumulation leads to excitotoxicity due to over-activation of NMDARs and leads to neuronal apoptosis (Rossi et al., 2000; Simon et al., 1984). Interestingly, NMDAR antagonists failed clinically to show neuroprotective effects or worsened stroke outcomes in patients (Davis et al., 2000; Sacco et al., 2001; Albers 1995, 2001). Hence, blocking NMDARs is detrimental as these receptors are also essential for physiologic functions. Neuronal survival displays an inverted U-shaped curve with respect to NMDAR activity, where physiologic activation during development promotes neuronal survival (Pearce et al., 1987).

Neuronal excitability after a stroke exhibits a yin and yang phase, where excess glutamate in the acute phase is deleterious. However, during the chronic phase, the peri-infarct tissue displays a marked increase in extracellular γ-aminobutyric acid (GABA) levels due to the loss of GABA transporter GAT-3(Clarkson et al., 2010). Notably, administration of L655,708, a benzodiazepine inverse agonist specific to the extrasynaptic GABAAR, produced early and sustained functional gains. Additionally, increasing baseline glutamatergic excitability during the chronic phase through direct current stimulation of the peri-infarct region improved the use of the affected limb in patients after stroke (Hummel and Cohen, 2006). Hence, counteracting the hypo-excitability caused by heightened inhibition, could potentially promote recovery when initiated during the chronic phase. Therefore, we hypothesized that enhancing brain excitability with PbTx-2 during the period of recovery and reorganization could potentially promote neurological recovery.

We selected the photothrombotic stroke model because it produces a localized infarct and is highly advantageous for detailed analysis of cells and functional studies (Labat-gest and Tomasi, 2013). The effect of photothrombotic stroke on fine motor deficits, assessed by pasta matrix reach task and foot fault task, appears to be both pervasive and persistent, because 6 days post stroke, vehicle-treated animals displayed a profound deficit in task performance. We found that a single PbTx-2 treatment applied 5 days post-stroke was sufficient to promote stroke recovery and that these beneficial effects may be mediated by the enhancement of synaptic plasticity and neuronal excitability. These effects of PbTx-2 on neuronal plasticity in the peri-infarct region are consistent with previous report in that neuronal activity affects structural plasticity in vivo through NMDAR-triggered intracellular signaling events (Sin WC et al., 2002).

Our results demonstrate a functional deficit after inducing stroke and reversal of this deficit by PbTx-2 suggest that stroke induced motor deficits might be especially responsive to cortical excitability during the recovery phase of stroke. Currently, the only treatment post-stroke is tPA, which must be administered within the first few hours post-infarct. Considering that occupational and physical therapy are the standard of care for stroke recovery, our results have identified a novel pharmacotherapy to accelerate recovery. Our data suggests that enhancing cortical excitability during the same time frame important for plasticity and recovery is promising to reduce the severity of stroke disability. Additionally, this strategy is more effective because it is applicable much later than current treatment options after stroke onset.

BIBLIOGRAPHY

Adams, H. P., Bendixen, B. H., Kappelle, L. J., Biller, J., Love, B. B., Gordon, D. L., & Marsh, E. E. (1993). Classification of subtype of acute ischemic stroke. Definitions for use in a multicenter clinical trial. TOAST. Trial of Org 10172 in Acute Stroke Treatment. *Stroke*, *24*(1), 35–41. doi: 10.1161/01.str.24.1.35.

Auer, P. L., Nalls, M., Meschia, J. F., Worrall, B. B., Longstreth, W. T., Seshadri, S., … Rich, S. S. (2015). Rare and Coding Region Genetic Variants Associated With Risk of Ischemic Stroke. *JAMA Neurology*, *72*(7), 781. doi: 10.1001/jamaneurol.2015.0582.

Baden, D.G. (1989). Brevetoxins: Unique polyether dinoflagellate toxins. *FASEB journal : official publication of the Federation of American Societies for Experimental Biology*, 3(7), 1807-17. Doi: 10.1096/fasebj.3.7.2565840.

Baden, D. G., Bourdelais, A. J., Jacocks, H., Michelliza, S., & Naar, J. (2005). Natural and Derivative Brevetoxins: Historical Background, Multiplicity, and Effects. *Environmental Health Perspectives*, *113*(5), 621–625. doi: 10.1289/ehp.7499

Balkaya, M., Kröber, J. M., Rex, A., & Endres, M. (2013). Assessing Post-Stroke Behavior in Mouse Models of Focal Ischemia. *Journal of Cerebral Blood Flow & Metabolism*, *33*(3), 330–338. doi: 10.1038/jcbfm.2012.185

Barth, T. M., Jones, T. A., & Schallert, T. (1990). Functional subdivisions of the rat somatic sensorimotor cortex. *Behavioural Brain Research*, *39*(1), 73–95. doi: 10.1016/0166-4328(90)90122-u.

Bergles, D. E., Diamond, J. S., & Jahr, C. E. (1999). Clearance of glutamate inside the synapse and beyond. *Current Opinion in Neurobiology*, *9*(3), 293–298. doi: 10.1016/s0959-4388(99)80043-9.

Benjamin, E. J., Blaha, M. J., Chiuve, S. E., Cushman, M., Das, S. R., Deo, R., de Ferranti, S. D., Floyd, J., Fornage, M., Gillespie, C., Isasi, C. R., Jiménez, M. C., Jordan, L. C., Judd, S. E., Lackland, D., Lichtman, J. H., Lisabeth, L., Liu, S., Longenecker, C. T., Mackey, R. H., … American Heart Association Statistics Committee and Stroke Statistics Subcommittee (2017). Heart Disease and Stroke Statistics-2017 Update: A Report From the American Heart Association. *Circulation*, *135*(10), e146–e603. https://doi.org/10.1161/CIR.0000000000000485.

Biernaskie, J., & Corbett, D. (2001). Enriched rehabilitative training promotes improved forelimb motor function and enhanced dendritic growth after focal ischemic injury. *The Journal of neuroscience : the official journal of the Society for Neuroscience*, *21*(14), 5272–5280. https://doi.org/10.1523/JNEUROSCI.21-14-05272.2001

Biernaskie, J., Szymanska, A., Windle, V., & Corbett, D. (2005). Bi-hemispheric contribution to functional motor recovery of the affected forelimb following focal ischemic brain injury in rats. *European Journal of Neuroscience*, *21*(4), 989–999. doi: 10.1111/j.1460-9568.2005.03899.x

Boller, F. (2004) Rational basis of rehabilitation following cerebral lesions: a review of the concept of cerebral plasticity. *Functional Neurology* 19(2), 65-72.

Bonfoco, E., Krainc, D., Ankarcrona, M., Nicotera, P., & Lipton, S. A. (1995). Apoptosis and necrosis: two distinct events induced, respectively, by mild and intense insults with N-methyl-D-aspartate or nitric oxide/superoxide in cortical cell cultures. *Proceedings of the National Academy of Sciences of the United States of America*, *92*(16), 7162–7166. https://doi.org/10.1073/pnas.92.16.7162

Bourne, J. N., & Harris, K. M. (2008). Balancing Structure and Function at Hippocampal Dendritic Spines. *Annual Review of Neuroscience*, *31*(1), 47–67. doi: 10.1146/annurev.neuro.31.060407.125646

Brown, C. E., Aminoltejari, K., Erb, H., Winship, I. R., & Murphy, T. H. (2009). In Vivo Voltage-Sensitive Dye Imaging in Adult Mice Reveals That Somatosensory Maps Lost to Stroke Are Replaced over Weeks by New Structural and Functional Circuits with Prolonged Modes of Activation within Both the Peri-Infarct Zone and Distant Sites. *Journal of Neuroscience*, *29*(6), 1719–1734. doi: 10.1523/jneurosci.4249-08.2009

Cargnello, M., & Roux, P. P. (2011). Activation and function of the MAPKs and their substrates, the MAPK-activated protein kinases. *Microbiology and molecular biology reviews : MMBR*, *75*(1), 50–83. https://doi.org/10.1128/MMBR.00031-10.

Carmichael S. T. (2016). The 3 Rs of Stroke Biology: Radial, Relayed, and Regenerative. *Neurotherapeutics : the journal of the American Society for Experimental NeuroTherapeutics*, *13*(2), 348–359. https://doi.org/10.1007/s13311-015-0408-0.

Candenas, L., Seda, M., Noheda, P., Buschmann, H., Cintado, C.G., Martin, J.D., Pinto, F. M. (2006). Molecular diversity of voltage-gated sodium channel alpha and beta subunit mRNAs in human tissues. *European journal of pharmacology*, 541(1-2), 9-16. Doi: 10.1016/j.ejphar.2006.04.025.

Cantrell, A. R., & Catterall, W. A. (2001). Neuromodulation of Na channels: An unexpected form of cellular platicity. *Nature Reviews Neuroscience*, *2*(6), 397–407. doi: 10.1038/35077553.

Carty, C. L., Keene, K. L., Cheng, Y. C., Meschia, J. F., Chen, W. M., Nalls, M., Bis, J. C., Kittner, S. J., Rich, S. S., Tajuddin, S., Zonderman, A. B., Evans, M. K., Langefeld, C. D., Gottesman, R., Mosley, T. H., Shahar, E., Woo, D., Yaffe, K., Liu, Y., Sale, M. M., … COMPASS and METASTROKE Consortia (2015). Meta-Analysis of Genome-Wide Association Studies Identifies Genetic Risk Factors for Stroke in African Americans. *Stroke*, *46*(8), 2063–2068. https://doi.org/10.1161/STROKEAHA.115.009044

Campbell, B.C.V., Mitchell, P.J., Kleinig, T.J., Dewey, H.M., Churilov, L., Yassi, N., Yan, B., Dowling, R.J., Parsons, M.W., Oxley, T.J., Wu, T.Y., Brooks, M., Simpson, M.A., Miteff, F., Levi, C.R., Krause, M., Harrington, T.J., Faulder, K.C., Steinfort, B.S., Priglinger, M., …EXTEND-IA Investigators (2015). Endovascular therapy for ischemic stroke with perfusion-imaging selection. *New*

England Journal of Medicine, 372 (11),1009-1018. DOI: 10.1056/NEJMoa1414792.

Catterall, W. A. (2000). From Ionic Currents to Molecular Mechanisms. *Neuron*, *26*(1), 13–25. doi: 10.1016/s0896-6273(00)81133-2.

Chang, F., Steelman, L.S., Lee, J.T., Shelton, J.G., Navolanic, P.M., Blalock, W.L., Franklin, R.A., McCubrey, J.A., (2003). Signal transduction mediated by the Ras/Raf/MEK/ERK pathway from cytokine receptors to transcription factors: potential targeting for therapeutic intervention. *Leukemia*, 17(7), 1263–1293. doi:10.1038/sj.leu.2402945.

Chang, P., & Prabhakaran, S. (2017). Recent advances in the management of acute ischemic stroke. *F1000Research*, *6*, 484. doi: 10.12688/f1000research.9191.1.

Clark, T. (2000). Chromatography: Thin-Layer (Planar) | Radioactivity detection. *Encylopedia of Separation Science*, 899-906. https://doi.org/10.1016/B0-12-226770-2/03081-7.

Clarkson, A.N., Huang, B.S., Macisaac, S.E., Mody, I., & Carmichael, S.T. (2010) Reducing excessive GABA-mediated tonic inhibition promotes functional recovery after stroke. *Nature* 468(7321), 305-309. doi: 10.1038/nature09511.

Clements, J., & Westbrook, G. (1991). Activation kinetics reveal the number of glutamate and glycine binding sites on the N-methyl-d-aspartate receptor. *Neuron*, *7*(4), 605–613. doi: 10.1016/0896-6273(91)90373-8

Collingridge, G. L., Isaac, J. T. R., & Wang, Y. T. (2004). Receptor trafficking and synaptic plasticity. *Nature Reviews Neuroscience*, *5*(12), 952–962. doi: 10.1038/nrn1556

Curcio, M., Salazar, I. L., Mele, M., Canzoniero, L. M., & Duarte, C. B. (2016). Calpains and neuronal damage in the ischemic brain: The swiss knife in synaptic injury. *Progress in Neurobiology*, *143*, 1–35. doi: 10.1016/j.pneurobio.2016.06.001.

Dangi, S., Chen, F.M., Shapiro, P., (2006). Activation of extracellular signal-regulated kinase (ERK) in G2 phase delays mitotic entry through p21CIP1. *Cell Proliferation*, 39(4), 261–279. doi:10.1111/j.1365-2184.2006.00388.x.

Dietrich, W. D., Watson, B. D., Busto, R., Ginsberg, M. D., & Bethea, J. R. (1987). Photochemically induced cerebral infarction. *Acta Neuropathologica*, *72*(4), 315–325. doi: 10.1007/bf00687262.

Dirnagl, U., Iadecola, C., & Moskowitz, M. A. (1999). Pathobiology of ischaemic stroke: an integrated view. *Trends in Neurosciences*, *22*(9), 391–397. doi: 10.1016/s0166-2236(99)01401-0.

Diss, J.K., Fraser, S.P., Djamgoz, M.B. (2004). Voltage-gated Na+ channels: multiplicity of expression, plasticity, functional implications and pathophysiological aspects. *European Biophysics Journal*. 33(3), 180-93. Doi: 10.1007/s00249-004-0389-0.

Dobkin, B. H., & Carmichael, S. T. (2016). The Specific Requirements of Neural Repair Trials for Stroke. *Neurorehabilitation and neural repair*, *30*(5), 470–478. https://doi.org/10.1177/1545968315604400

Donnan GA, Fisher M, Macleod M, Davis SM. Stroke. *Lancet.* 2008;371(9624):1612–23

Du, J., Feng, L., Yang, F., & Lu, B. (2000). Activity- and Ca2 -Dependent Modulation of Surface Expression of Brain-Derived Neurotrophic Factor Receptors in Hippocampal Neurons. *Journal of Cell Biology, 150*(6), 1423–1434. doi: 10.1083/jcb.150.6.1423

Eliasson, M. J. L., Huang, Z., Ferrante, R. J., Sasamata, M., Molliver, M. E., Snyder, S. H., & Moskowitz, M. A. (1999). Neuronal Nitric Oxide Synthase Activation and Peroxynitrite Formation in Ischemic Stroke Linked to Neural Damage. *The Journal of Neuroscience, 19*(14), 5910–5918. doi: 10.1523/jneurosci.19-14-05910.1999

Elston, G.N. (2007). Primates. *Evolution of Nervous Systems*, 18. doi: 10.1016/b0-12-370878-8/09010-8

Feng, G., Mellor, R. H., Bernstein, M., Keller-Peck, C., Nguyen, Q. T., Wallace, M., … Sanes, J. R. (2000). Imaging Neuronal Subsets in Transgenic Mice Expressing Multiple Spectral Variants of GFP. *Neuron, 28*(1), 41–51. doi: 10.1016/s0896-6273(00)00084-2

Finsterer J. (2010). Management of cryptogenic stroke. *Acta Neurologica Belgica*. 110 (2), 135-47.

Fleming, L. E., Kirkpatrick, B., Backer, L. C., Bean, J. A., Wanner, A., Dalpra, D., … Baden, D. G. (2005). Initial Evaluation of the Effects of Aerosolized Florida Red Tide Toxins (Brevetoxins) in Persons with Asthma. *Environmental Health Perspectives, 113*(5), 650–657. doi: 10.1289/ehp.7500.

Fluri, F., Schuhmann, M & Kleinschnitz, C. (2015). Animal models of ischemic stroke and their application in clinical research. *Drug Design, Development and Therapy*, 3445. doi: 10.2147/dddt.s56071.

Forrest, M. P., Parnell, E., & Penzes, P. (2018). Dendritic structural plasticity and neuropsychiatric disease. *Nature Reviews Neuroscience*, *19*(4), 215–234. doi: 10.1038/nrn.2018.16.

Fremeau, R. T., Troyer, M. D., Pahner, I., Nygaard, G. O., Tran, C. H., Reimer, R. J., … Edwards, R. H. (2001). The Expression of Vesicular Glutamate Transporters Defines Two Classes of Excitatory Synapse. *Neuron*, *31*(2), 247–260. doi: 10.1016/s0896-6273(01)00344-0.

Fremeau, R. T., Burman, J., Qureshi, T., Tran, C. H., Proctor, J., Johnson, J., … Edwards, R. H. (2002). The identification of vesicular glutamate transporter 3 suggests novel modes of signaling by glutamate. *Proceedings of the National Academy of Sciences*, *99*(22), 14488–14493. doi: 10.1073/pnas.222546799.

Fukuoka, T., Noguchi, K. (2011). Comparative study of voltage-gated sodium channel alpha-subunits in non-overlapping four neuronal populations in the rat dorsal root ganglion. *Neuroscience research,* 70(2), 164-71. doi:10.1016/j.neures.2011.01.020.

Gardner, M. J., & Altman, D. G. (1986). Confidence intervals rather than P values: estimation rather than hypothesis testing. *Bmj*, *292*(6522), 746–750. doi: 10.1136/bmj.292.6522.746.

Ganguly, K., & Poo, M.-M. (2013). Activity-Dependent Neural Plasticity from Bench to Bedside. *Neuron*, *80*(3), 729–741. doi: 10.1016/j.neuron.2013.10.028

Gawley, R., Rein, K., Jeglitsch, G., Adams, D., Theodorakis, E., Tiebes, J., Nicolaou, K., & Baden, D. (1995). The relationship of brevetoxin 'length' and A-ring functionality to binding and activity in neuronal sodium channels. *Chemistry & Biology*, 2(8), pp.533-541.

George, J., Dravid, S. M., Prakash, A., Xie, J., Peterson, J., Jabba, S. V., Baden, D. G., & Murray, T. F. (2009). Sodium channel activation augments NMDA receptor function and promotes neurite outgrowth in immature cerebrocortical neurons. *The Journal of neuroscience : the official journal of the Society for Neuroscience*, *29*(10), 3288–3301. https://doi.org/10.1523/JNEUROSCI.6104-08.2009.

Gerloff, C., Bushara, K., Sailer, A., Wassermann, E. M., Chen, R., Matsuoka, T., … Hallett, M. (2006). Multimodal imaging of brain reorganization in motor areas of the contralesional hemisphere of well recovered patients after capsular stroke. *Brain*, *129*(3), 791–808. doi: 10.1093/brain/awh713.

Goldin, A. L., Barchi, R. L., Caldwell, J. H., Hofmann, F., Howe, J. R., Hunter, J. C., … Catterall, W. A. (2000). Nomenclature of Voltage-Gated Sodium Channels. *Neuron*, *28*(2), 365–368. https://doi.org/10.1016/s0896-6273(00)00116-1.

Gras, C., Herzog, E., Bellenchi, G. C., Bernard, V., Ravassard, P., Pohl, M., … Mestikawy, S. E. (2002). A Third Vesicular Glutamate Transporter Expressed by

Cholinergic and Serotoninergic Neurons. *The Journal of Neuroscience*, *22*(13), 5442–5451. doi: 10.1523/jneurosci.22-13-05442.2002.

Gretarsdottir, S., Thorleifsson, G., Manolescu, A., Styrkarsdottir, U., Helgadottir, A., Gschwendtner, A., … Stefansson, K. (2008). Risk variants for atrial fibrillation on chromosome 4q25 associate with ischemic stroke. *Annals of Neurology*, *64*(4), 402–409. doi: 10.1002/ana.21480.

Groc, L., Heine, M., Cousins, S. L., Stephenson, F. A., Lounis, B., Cognet, L., & Choquet, D. (2006). NMDA receptor surface mobility depends on NR2A-2B subunits. *Proceedings of the National Academy of Sciences*, *103*(49), 18769–18774. doi: 10.1073/pnas.0605238103.

Hall, M.J., Levant, S., DeFrances, C.J. (2012). Hospitalization for stroke in U.S. hospitals, 1989–2009. *NCHS data brief*, 95, 1-8.

Heinrich, A., Andó, R., Túri, G., Rózsa, B., & Sperlágh, B. (2012). K depolarization evokes ATP, adenosine and glutamate release from glia in rat hippocampus: a microelectrode biosensor study. *British Journal of Pharmacology*, *167*(5), 1003–1020. doi: 10.1111/j.1476-5381.2012.01932.x

Hodgkin, A. L., & Huxley, A. F. (1952). A quantitative description of membrane current and its application to conduction and excitation in nerve. *The Journal of Physiology*, *117*(4), 500–544. doi: 10.1113/jphysiol.1952.sp004764.

Ho, J., Tumkaya, T., Aryal, S., Choi, H., & Claridge-Chang, A. (2019). Moving beyond P values: data analysis with estimation graphics. *Nature Methods*, *16*(7), 565–566. doi: 10.1038/s41592-019-0470-3.

Howard, G., Anderson, R., Johnson, N. J., Sorlie, P., Russell, G., & Howard, V. J. (1997). Evaluation of Social Status as a Contributing Factor to the Stroke Belt Region of the United States. *Stroke*, *28*(5), 936–940. doi: 10.1161/01.str.28.5.936.

Hummel, F.C., & Cohen, L.G. (2006). Non-invasive brain stimulation: a new strategy to improve neurorehabilitation after stroke? 5(8), 708-712. doi.org/10.1016/S1474-4422(06)70525-7.

Ikegaya,Y., Kim, J.A., Baba, M., Iwatsubo, T., Nishiyama, N., & Matsuki, N. (2001) Rapid and reversible changes in dendrite morphology and synaptic efficacy following NMDA receptor activation: implication for a cellular defense against excitotoxicity. *Journal of Cell Science.* 114 (22), 4083-4093.

Ikram, M., Seshadri, S., & Bis, J. (2009). Genomewide Association Studies of Stroke. *Journal of Vascular Surgery*, *50*(2), 467. doi: 10.1016/j.jvs.2009.06.027.

Ishida, H., Nozawa, A., Totoribe, K., et al. (1995). Brevetoxin B1, a new polyether marine toxin from the New Zealand shellfish, Austrovenus stutchburyi. *Tetrahedron Letters*, 36:725–728.

Jeglitsch, G., Rein, K.S., Baden, D.G., & Adams, D.J. (1998). Brevetoxin-3 (PbTx-3) and its derivatives modulate single tetrodotoxin-sensitive sodium channels in rat sensory neurons. *The Journal of pharmacology and experimental therapeutics, 284 2*, 516-25.

Johnson, J. W., & Ascher, P. (1987). Glycine potentiates the NMDA response in cultured mouse brain neurons. *Nature*, *325*(6104), 529–531. doi: 10.1038/325529a0.

Jones, T. A., & Schallert, T. (1992). Overgrowth and pruning of dendrites in adult rats recovering from neocortical damage. *Brain Research*, *581*(1), 156–160. doi: 10.1016/0006-8993(92)90356-e.

Kleckner, N., & Dingledine, R. (1988). Requirement for glycine in activation of NMDA-receptors expressed in Xenopus oocytes. *Science, 241*(4867), 835–837. doi: 10.1126/science.2841759.

Kobayashi, Y., & Lavenex, P. (2015). Neuroanatomy Methods in Humans and Animals☆. *Reference Module in Biomedical Sciences*. https://doi.org/10.1016/b978-0-12-801238-3.04682-1.

Komuro, H., & Rakic, P. (1993). Modulation of neuronal migration by NMDA receptors. *Science*, *260*(5104), 95–97. doi: 10.1126/science.8096653.

Konur, S., & Ghosh, A. (2005). Calcium Signaling and the Control of Dendritic Development. *Neuron*, *46*(3), 401–405. doi: 10.1016/j.neuron.2005.04.022.

Kristián Tibor, & Siesjö Bo K. (1998). Calcium in Ischemic Cell Death. *Stroke*, *29*(3), 705–718. doi: 10.1161/01.str.29.3.705.

Labat-Gest, V., & Tomasi, S. (2013). Photothrombotic Ischemia: A Minimally Invasive and Reproducible Photochemical Cortical Lesion Model for Mouse Stroke Studies. *Journal of Visualized Experiments*, (76). doi: 10.3791/50370.

Lai, H. C., & Jan, L. Y. (2006). The distribution and targeting of neuronal voltage-gated ion channels. *Nature Reviews Neuroscience*, *7*(7), 548–562. doi: 10.1038/nrn1938.

Lau, A., & Tymianski, M. (2010). Glutamate receptors, neurotoxicity and neurodegeneration. *Pflügers Archiv - European Journal of Physiology*, *460*(2), 525–542. doi: 10.1007/s00424-010-0809-1.

Li, J., & Mooney, D. J. (2016). Designing hydrogels for controlled drug delivery. *Nature Reviews Materials*, *1*(12). doi: 10.1038/natrevmats.2016.

Lim, D. H., Ledue, J. M., Mohajerani, M. H., & Murphy, T. H. (2014). Optogenetic Mapping after Stroke Reveals Network-Wide Scaling of Functional Connections and Heterogeneous Recovery of the Peri-Infarct. *The Journal of Neuroscience*, *34*(49), 16455–16466. doi: 10.1523/jneurosci.3384-14.2014.

Lipton, S. A., & Nakanishi, N. (1999). Shakespeare in love—with NMDA receptors? *Nature Medicine*, *5*(3), 270–271. doi: 10.1038/6481.

Liu, Y., & Rouiller, E. M. (1999). Mechanisms of recovery of dexterity following unilateral lesion of the sensorimotor cortex in adult monkeys. *Experimental Brain Research*, *128*(1-2), 149–159. doi: 10.1007/s002210050830.

Lopez, A. D., Mathers, C. D., Ezzati, M., Jamison, D. T., & Murray, C. J. (2006). Global and regional burden of disease and risk factors, 2001: systematic analysis of population health data. *The Lancet*, *367*(9524), 1747–1757. doi: 10.1016/s0140-6736(06)68770-9.

Lyerly, M. J., Albright, K. C., Boehme, A. K., Shahripour, R. B., Houston, J. T., Rawal, P. V., Kapoor, N., Alvi, M., Sisson, A., Alexandrov, A. W., & Alexandrov, A. V. (2013). The Potential Impact of Maintaining a 3-Hour IV Thrombolysis Window:

How Many More Patients can we Safely Treat?. *Journal of neurological disorders & stroke*, *1*(2), 1015.

Malik, R., Chauhan, G., Traylor, M., Sargurupremraj, M., Okada, Y., Mishra, A., Rutten-Jacobs, L., Giese, A. K., van der Laan, S. W., Gretarsdottir, S., Anderson, C. D., Chong, M., Adams, H., Ago, T., Almgren, P., Amouyel, P., Ay, H., Bartz, T. M., Benavente, O. R., Bevan, S., … Dichgans, M. (2018). Multiancestry genome-wide association study of 520,000 subjects identifies 32 loci associated with stroke and stroke subtypes. *Nature genetics*, *50*(4), 524–537. doi.org/10.1038/s41588-018-0058-3.

Mani S, Mutha KP, Sainburg LR (2013) Contralesional motor deficits after unilateral stroke reflect hemisphere-specific control mechanisms. Brain 4: 1288- 1303

Mattson, M. P. (2003). Excitotoxic and Excitoprotective Mechanisms: Abundant Targets for the Prevention and Treatment of Neurodegenerative Disorders. *NeuroMolecular Medicine*, *3*(2), 65–94. doi: 10.1385/nmm:3:2:65.

Matus, A. (2000). Actin-Based Plasticity in Dendritic Spines. *Science*, *290*(5492), 754–758. doi: 10.1126/science.290.5492.754.

Merino, J. G., & Warach, S. (2010). Imaging of acute stroke. *Nature Reviews Neurology*, *6*(10), 560–571. doi: 10.1038/nrneurol.2010.129.

Modo, M., Stroemer, R., Tang, E., Veizovic, T., Sowniski, P., & Hodges, H. (2000). Neurological sequelae and long-term behavioural assessment of rats with transient middle cerebral artery occlusion. *Journal of Neuroscience Methods*, *104*(1), 99–109. doi: 10.1016/s0165-0270(00)00329-0.

Monyer, H., Sprengel, R., Schoepfer, R., Herb, A., Higuchi, M., Lomeli, H., … Seeburg, P. H. (1992). Heteromeric NMDA Receptors: Molecular and Functional Distinction of Subtypes. *Science*, *256*(5060), 1217–1221. doi: 10.1126/science.256.5060.1217

Morris, P. D., Campbell, D. S., Taylor, T. J., & Freeman, J. I. (1991). Clinical and epidemiological features of neurotoxic shellfish poisoning in North Carolina. *American Journal of Public Health*, *81*(4), 471–474. doi: 10.2105/ajph.81.4.471.

Moskowitz, M. A., Lo, E. H., & Iadecola, C. (2010). The Science of Stroke: Mechanisms in Search of Treatments. *Neuron*, *67*(2), 181–198. doi: 10.1016/j.neuron.2010.07.002.

Mozaffarian, D., Benjamin, E. J., Go, A. S., Arnett, D. K., Blaha, M. J., Cushman, M., Das, S. R., de Ferranti, S., Després, J. P., Fullerton, H. J., Howard, V. J., Huffman, M. D., Isasi, C. R., Jiménez, M. C., Judd, S. E., Kissela, B. M., Lichtman, J. H., Lisabeth, L. D., Liu, S., ... on behalf of the American Heart Association Statistics Committee and Stroke Statistics Subcommittee (2016). Heart disease and stroke statistics-2016 update a report from the American Heart Association. *Circulation*, *133*(4), e38-e48. doi.org/10.1161/CIR.0000000000000350.

Mozaffarian, D., Benjamin, E. J., Go, A. S., Arnett, D. K., Blaha, M. J., Cushman, M., … Turner, M. B. (2015). Heart Disease and Stroke Statistics—2015 Update. *Circulation*, *131*(4). doi: 10.1161/cir.0000000000000152.

Murphy, T. H., & Corbett, D. (2009). Plasticity during stroke recovery: from synapse to behaviour. *Nature Reviews Neuroscience*, *10*(12), 861–872. doi: 10.1038/nrn2735.

National Institute of Neurological Disorders and Stroke (U.S.). (2004). *Stroke: Hope through research*. Bethesda, MD: National Institute of Neurological Disorders and Stroke, National Institutes of Health.

Nyitrai, G., Kekesi, K.A., & Juhasz, G. (2006). Extracellular level of GABA and Glu: in vivo microdialysis-HPLC measurements. *Current Topics in Medicinal Chemistry*, 6(10), 935-940. 10.2174/156802606777323674.

Odonnell, M. J., Xavier, D., Liu, L., Zhang, H., Chin, S. L., Rao-Melacini, P., … Yusuf, S. (2010). Risk factors for ischaemic and intracerebral haemorrhagic stroke in 22 countries (the INTERSTROKE study): a case-control study. *The Lancet*, *376*(9735), 112–123. doi: 10.1016/s0140-6736(10)60834-3.

Onkal, R., Mattis, J.H., Fraser, S.P, Diss, J.K., Shao, D., Okuse, K., & Djamgoz, M.B. (2008). Alternative splicing of Nav1.5: an electrophysiological comparison of 'neonatal' and 'adult' isoforms and critical involvement of a lysine residue. *Journal of Cell Physiology*, 216(3), 716-26. doi:10.1002/jcp.21451.

Pappalardo, L. W., Black, J. A., & Waxman, S. G. (2016). Sodium channels in astroglia and microglia. *Glia*, *64*(10), 1628–1645. https://doi.org/10.1002/glia.22967.

Patneau, D., & Mayer, M. (1990). Structure-activity relationships for amino acid transmitter candidates acting at N-methyl-D-aspartate and quisqualate receptors. *The Journal of Neuroscience*, *10*(7), 2385–2399. doi: 10.1523/jneurosci.10-07-02385.1990

Pearce, I.A., Cambray, D.M. & Burgoyne, R.D. (1987). Glutamate acting on NMDA receptors stimulates neurite outgrowth from cerebellar granule cells. *FEBS Letters*. 223(1), 143–147. doi.org/10.1016/0014-5793(87)80525-2.

Petit, T. L., Leboutillier, J. C., Gregorio, A., & Libstug, H. (1988). The pattern of dendritic development in the cerebral cortex of the rat. *Developmental Brain Research*, *41*(1-2), Phillis, J., & O'Regan, M. (2003). Characterization of modes of release of amino acids in the ischemic/reperfused rat cerebral cortex. *Neurochemistry International*, *43*(4-5), 461–467. doi: 10.1016/s0197-0186(03)00035-4.

Plakas, S. M., & Dickey, R. W. (2010). Advances in monitoring and toxicity assessment of brevetoxins in molluscan shellfish. *Toxicon*, *56*(2), 137–149. doi: 10.1016/j.toxicon.2009.11.007209–219. doi: 10.1016/0165-3806(88)90183-6.

Poli, M.A., Mende, T.J., Baden, D.G. (1986). Brevetoxins, unique activators of voltage sensitive sodium channels, bind to specific sites in rat brain synaptosomes. *Molecular Pharmacology*, 30(2), 129-135.

Poli, M. A., Musser, S. M., Dickey, R. W., Eilers, P. P., & Hall, S. (2000). Neurotoxic shellfish poisoning and brevetoxin metabolites: a case study from Florida. *Toxicon*, *38*(7), 981–993. doi: 10.1016/s0041-0101(99)00191-9.

Portera-Cailliau, C., Pan, D. T., & Yuste, R. (2003). Activity-Regulated Dynamic Behavior of Early Dendritic Protrusions: Evidence for Different Types of

Dendritic Filopodia. *The Journal of Neuroscience*, *23*(18), 7129–7142. doi: 10.1523/jneurosci.23-18-07129.2003.

Powers, W. J., Derdeyn, C. P., Biller, J., Coffey, C. S., Hoh, B. L., Jauch, E. C., … Yavagal, D. R. (2015). 2015 American Heart Association/American Stroke Association Focused Update of the 2013 Guidelines for the Early Management of Patients With Acute Ischemic Stroke Regarding Endovascular Treatment. *Stroke*, *46*(10), 3020–3035. doi: 10.1161/str.0000000000000074.

Racca, C., Stephenson, F. A., Streit, P., Roberts, J. D., & Somogyi, P. (2000). NMDA receptor content of synapses in stratum radiatum of the hippocampal CA1 area. *The Journal of neuroscience : the official journal of the Society for Neuroscience*, *20*(7), 2512–2522. https://doi.org/10.1523/JNEUROSCI.20-07-02512.2000.

Rannikmäe, K., Woodfield, R., Anderson, C. S., Charidimou, A., Chiewvit, P., Greenberg, S. M., … Sudlow, C. L. (2016). Reliability of intracerebral hemorrhage classification systems: A systematic review. *International Journal of Stroke*, *11*(6), 626–636. https://doi.org/10.1177/1747493016641962.

Rogers, D. C., Campbell, C. A., Stretton, J. L., & Mackay, K. B. (1997). Correlation Between Motor Impairment and Infarct Volume After Permanent and Transient Middle Cerebral Artery Occlusion in the Rat. *Stroke*, *28*(10), 2060–2066. doi: 10.1161/01.str.28.10.2060.

Rose, C.R., Kovalchuk, Y., Eilers, J., & Konnerth A. (1999). Two-photon Na+ imaging in spines and fine dendrites of central neurons. *Pflugers Archiv- European Journal of Physiology*, 439(1-2),201-7. doi.org/10.1007/s004249900123

Rose, C. R., & Konnerth, A. (2001). NMDA Receptor-Mediated Na Signals in Spines and Dendrites. *The Journal of Neuroscience*, *21*(12), 4207–4214. doi: 10.1523/jneurosci.21-12-04207.2001.

Salter, M. W. (1999). A pinch of salt for NMDA receptors. *Molecular Psychiatry*, *4*(3), 209–211. doi: 10.1038/sj.mp.4000540.

Saver, J.L., Goyal, M., Lugt, A.V., Menon, B.K., Majoie, C.B., Dippel, D.W., Campbell, B.C., Nogueira, R.G., Demchuk, A.M., Tomasello, A., Cardona, P., Devlin, T.G., Frei, D.F., Rochemont, R.D., Berkhemer, O.A., Jovin, T.G., Siddiqui, A.H., Zwam, W.H., Davis, S.M., Castaño, C., Sapkota, B.L., Fransen, P.S., Molina, C., Oostenbrugge, R.J., Chamorro, Á., Lingsma, H.F., Silver, F.L., Donnan, G.A., Shuaib, A., Brown, S.T., Stouch, B.C., Mitchell, P.J., Davalos, A., Roos, Y.B., & Hill, M.D. (2016). Time to Treatment With Endovascular Thrombectomy and Outcomes From Ischemic Stroke: A Meta-analysis. *JAMA, 316 12*, 1279-88 . doi:10.1001/jama.2016.13647.

Schaar, K. L., Brenneman, M. M., & Savitz, S. I. (2010). Functional assessments in the rodent stroke model. *Experimental & translational stroke medicine*, *2*(1), 13. https://doi.org/10.1186/2040-7378-2-13

Schäbitz Wolf-Rüdiger, Steigleder, T., Cooper-Kuhn, C. M., Schwab, S., Sommer, C., Schneider, A., & Kuhn, H. G. (2007). Intravenous Brain-Derived Neurotrophic

Factor Enhances Poststroke Sensorimotor Recovery and Stimulates Neurogenesis. *Stroke, 38*(7), 2165–2172. doi: 10.1161/strokeaha.106.477331.

Schaller, K.L., Caldwell, J.H. (2000). Developmental and regional expression of sodium channel isoform NaCh6 in the rat central nervous system. *Journal of comparative neurology*, 420, 84-97. Doi: 10.1002/(SICI)1096-9861(20000424)420:1%3c84::AID-CNE6%3e3.0.CO;2-9.

Schaller, K.L., Caldwell, J.H. (2003). Expression and distribution of voltage-gated sodium channels in the cerebellum. *Cerebellum*, 2(1), 2-9. doi:10.1080/14734220309424. PMID:12882229.

Schallert, T., & Woodlee, M.T. (2005) The Behavior of the Laboratory Rat: A Handbook with Tests. *Oxford University Press*. 129–140.

Schunkert, H., Götz, A., Braund, P., McGinnis, R., Tregouet, D. A., Mangino, M., Linsel-Nitschke, P., Cambien, F., Hengstenberg, C., Stark, K., Blankenberg, S., Tiret, L., Ducimetiere, P., Keniry, A., Ghori, M. J., Schreiber, S., El Mokhtari, N. E., Hall, A. S., Dixon, R. J., Goodall, A. H., … Cardiogenics Consortium (2008). Repeated replication and a prospective meta-analysis of the association between chromosome 9p21.3 and coronary artery disease. *Circulation*, *117*(13), 1675–1684. doi.org/10.1161/CIRCULATIONAHA.107.730614.

Spruston, N. (2008). Pyramidal neurons: dendritic structure and synaptic integration. *Nature Reviews. Neuroscience*. 9(3), 206–221. doi: 10.1038/nrn2286.

Takeshima, Y., Nakamura, M., Miyake, H., Tamaki, R., Inui, T., Horiuchi, K., … Nakase, H. (2011). Neuroprotection With Intraventricular Brain-Derived

Neurotrophic Factor in Rat Venous Occlusion Model. *Neurosurgery*, *68*(5), 1334–1341. doi: 10.1227/neu.0b013e31820c048e.

Trainer, V.L., Baden, D.G., Catterall, W.A. (1994). Identification of the peptide components of the brevetoxin receptor site of rat brain sodium channels. *Journal of Biological Chemistry*, 269(31), 19904-19909.

Traynelis, S. F., Wollmuth, L. P., Mcbain, C. J., Menniti, F. S., Vance, K. M., Ogden, K. K., … Dingledine, R. (2010). Glutamate Receptor Ion Channels: Structure, Regulation, and Function. *Pharmacological Reviews*, *62*(3), 405–496. doi: 10.1124/pr.109.002451

Triller, A., Cluzeaud, F., Pfeiffer, F., Betz, H., & Korn, H. (1985). Distribution of glycine receptors at central synapses: an immunoelectron microscopy study. *The Journal of Cell Biology*, *101*(2), 683–688. doi: 10.1083/jcb.101.2.683.

Tunik, M.G. (2011). Chapter 45. Food Poisoning. In: Hoffman RS, Nelson LS, Goldfrank LR, Howland MA, Lewin NA, Flomenbaum NE, eds. Goldfrank’s Toxicologic Emergencies. 9th ed. New York: McGraw-Hill, 668-681.

Ulbrich, M. H., & Isacoff, E. Y. (2008). Rules of engagement for NMDA receptor subunits. *Proceedings of the National Academy of Sciences*, *105*(37), 14163–14168. doi: 10.1073/pnas.0802075105.

Vacher, H., Mohapatra, D. P., & Trimmer, J. S. (2008). Localization and targeting of voltage-dependent ion channels in mammalian central neurons. *Physiological reviews*, *88*(4), 1407–1447. https://doi.org/10.1152/physrev.00002.2008.

Wang, J., Ou, S.W., Wang, Y.J., Kameyama, M., Kameyama, A., & Zong, Z.H. (2009). Analysis of four novel variants of Nav1.5/SCN5A cloned from the brain. *Neuroscience research.* 64(4), 339-47. doi:10.1016/j.neures.2009.04.003.

Watkins, J. C., & Evans, R. H. (1981). Excitatory Amino Acid Transmitters. *Annual Review of Pharmacology and Toxicology*, *21*(1), 165–204. doi: 10.1146/annurev.pa.21.040181.001121.

Watkins, S. M., Reich, A., Fleming, L. E., & Hammond, R. (2008). Neurotoxic shellfish poisoning. *Marine drugs*, *6*(3), 431–455. https://doi.org/10.3390/md20080021.

Whitaker, W.R., Faull, R.L., Waldvogel, H,J, Plumpton, C.J., Emson, P.C., & Clare, J.J. (2001). Comparative distribution of voltage-gated sodium channel proteins in human brain. *Brain Research. Molecular Brain Research.* 88(1-2), 37-53. 10.1016/s0169-328x(00)00289-8.

Whitaker, W.R., Clare, J.J., Powell, A.J., Chen, Y.H., Faull, R.L., Emson, P.C. (2000). Distribution of voltage-gated sodium channel alpha-subunit and beta-subunit mRNAs in human hippocampal formation, cortex, and cerebellum. *The journal of comparative neurology.* 422(1), 123-39. Doi: 10.1002/(sici)1096-9861(20000619)422:1<123::aid-cne8>3.0.co;2-x.

Wong, R. O. L., & Ghosh, A. (2002). Activity-dependent regulation of dendritic growth and patterning. *Nature Reviews Neuroscience, 3*(10), 803–812. doi: 10.1038/nrn941.

Wood, J., Baker N. (2001). Voltage-gated sodium channels. *Current Opinion in Pharmacology*, *1*(1), 17–21. doi: 10.1016/s1471-4892(01)00007-8.

Xu, J., Kurup, P., Zhang, Y., Goebel-Goody, S. M., Wu, P. H., Hawasli, A. H., … Lombroso, P. J. (2009). Extrasynaptic NMDA Receptors Couple Preferentially to Excitotoxicity via Calpain-Mediated Cleavage of STEP. *Journal of Neuroscience*, *29*(29), 9330–9343. doi: 10.1523/jneurosci.2212-09.2009.

Yu, F. H., & Catterall, W. A. (2003). Overview of the voltage-gated sodium channel family. *Genome Biology*, *4*(3), 207. doi: 10.1186/gb-2003-4-3-207.

Yu, F. H., Yarov-Yarovoy, V., Gutman, G. A., & Catterall, W. A. (2005). Overview of Molecular Relationships in the Voltage-Gated Ion Channel Superfamily. *Pharmacological Reviews*, *57*(4), 387–395. doi: 10.1124/pr.57.4.13.

Ziv, N. E., & Smith, S. J. (1996). Evidence for a Role of Dendritic Filopodia in Synaptogenesis and Spine Formation. *Neuron*, *17*(1), 91–102. doi: 10.1016/s0896-6273(00)80283-4.